Chair of Petroleum and Geothermal Energy Recovery

Master's Thesis

Slippage investigation and model development for Sucker-Rod-Pumps

Daniel Kochtik, BSc

September 2019

EIDESSTATTLICHE ERKLÄRUNG

Ich erkläre an Eides statt, dass ich die vorliegende Masterarbeit selbständig und ohne fremde Hilfe verfasst, andere als die angegebenen Quellen und Hilfsmittel nicht benutzt und die den benutzten Quellen wörtlich und inhaltlich entnommenen Stellen als solche erkenntlich gemacht habe.

Ich erkläre, dass ich die Richtlinien des Senats der Montanuniversität Leoben zu "Gute wissenschaftliche Praxis" gelesen, verstanden und befolgt habe.

Weiters erkläre ich, dass die elektronische und gedruckte Version der eingereichten wissenschaftlichen Abschlussarbeit formal und inhaltlich identisch sind.

Leoben, am. . . . .
                                                                                      (Unterschrift Daniel Kochtik BSc.)

Every model is an approximation.

Danksagung / Acknowledgment

Es war sehr schön, es hat mich sehr gefreut!

Kurzfassung

Niedrige, schwankende Ölpreise an der Börse und eine hohe Verwässerung der Produktion zwingen Ölkonzerne ihre Anlagen kontinuierlich zu optimieren, um den Anforderungen im Sinne einer hohen Effizienz gerecht zu werden.

Der Einsatz von effizienten Pumpsystemen in alten Ölfeldern ist ein Schritt in Richtung Optimierung der Ölförderungskette von der Lagerstätte bis hin zum Endkunden.

Gestängetiefpumpen sind auch heute noch eines der am häufigsten eingesetzten künstlichen Hebesystem in der Ölindustrie. Diese Pumpen stellen eine effiziente, einfache und solide Möglichkeit zur Erhöhung der Ölförderung dar. Einerseits ist dieses System technisch leicht an wechselnde Betriebsbedingungen anpassbar, andererseits ist der wirtschaftliche und ökologische Fußabdruck im Vergleich zu konkurrierenden Systemen relativ gering.

Aufgrund der Vielzahl der installierten Einheiten ist eine technisch-effiziente und ausfallsichere Konstruktion des Pumpsystems unerlässlich. Ein tiefgreifendes Verständnis der Vorgänge während des Pumpens ist für die kontinuierliche Optimierung des Pumpensystems von großer Bedeutung.

Dieser Arbeit präsentiert die Ergebnisse von volumetrischen Effizienztests, durchgeführt für verschiedene Betriebsbedingungen an dem Pumpenteststand der Montanuniversitaet Leoben. Es werden die Ergebnisse der verschiedenen Versuche zum Erreichen eines detaillierten Verständnisses der internen Verluste während des Pumpvorgangs vorgestellt.

Die Leckrate der Pumpe ist stark abhängig vom Differenzdruck und ebenso von der Hubzahl je Minute. Fünf verschiedene Kolben werden mit je drei unterschiedlichen Flüssigkeitstypen getestet. Die experimentellen Ergebnisse werden mit existierenden Leckagemodellen verglichen. Der Vergleich zeigt deutlich, dass die meisten der existierenden Leckagemodelle das Leckagevolumen um einen signifikanten Anteil unterschätzen.

Aus diesem Grund besteht die Notwendigkeit eines neuen Modells. Das neu entwickelte Modell unterscheidet sich im Ansatz der Messungen und im Resultat der Ergebnisse. Dieses Modell hilft nun Ingenieuren Schlupfverluste bis zu 38bar besser zu beschreiben.

Abstract

Low instable oil prices at the stock market and an increasing water cut force engineers to constantly improve and redesign their methods in order to optimize efficiency. The use of efficient artificial lift systems in old oil fields is a step forward to improve the value chain from reservoir to customer. To this day Sucker Rod Pumps are one of the most used artificial lift systems in the oil industry. These pumps represent a cost efficient and simple way to increase oil production. One the one hand this system is easily adjustable to chaning operating conditions and on the other hand has a good cost-effectiveness compared to other systems. Due to the high number of installed units it is essential to have a technical efficient and failsafe construction of the lift system. A deep understanding of the procedure of the pumping operation is vital for the continuous optimization.

This thesis presents the results of the research on the topic of volumetric efficiency for different operating conditions performed at the Pump Test Facility of Montanuniversitaet Leoben.

The different results of the test are illustrated in order to gain detailed understanding of internal losses durind the pumping operation. Slippage strongly depends on the differential pressure across the pump and the pumping speed. Five different plungers were tested with three different types of liquids. The experimental results were then compared with existing models. The results were then compared to existing slippage models. The comparison between those models clearly indicate the underestimation of the amount of slippage.

The reasons mentioned above show the necessity to develop a new equation. The result of several different theoretical approaches was than fitted to describe the measurements performed at the Pump Test Facility in Leoben. The new model differs in result and approach compared to the already existing models.

The new model helps engineers to calculate slippage up to 38bar pressure difference across the pump.

Contents

Contents

1. Introduction

1.1. Current Status - Necessity

The latest instabilities of the oil price at the stock market show the necessity of a profitable oil production system. In addition, high water cuts even increase the need of a well designed and profitable production system. Oil companies with major share on mature oil fields are constantly forced to optimize and adjust their facilities to the current needs regarding efficiency and profitability.

An important point in the oil production system is the proper design of an artificial lift system, which helps to produce low-pressure reservoirs. Sucker rod pumps are still one of the most common artificial lift systems.Due to their reliability and easiness to adjust to changing operating conditions. Furthermore, the economic and environmental footprint of sucker rod pumps are rather low compared to other artificial lift systems. Sucker rod pumps are positive displacement pumps, therefore even a not well designed system will produce a certain amount of fluid. But the high number of installed units makes it necessary to have an optimally designed and failure resistant system.

One of the most influencing factors of the efficiency of sucker rod pumps is the volumetric efficiency of the downhole pump.

The volumetric efficiency directly affects the maximum produceable amount of fluid. Losses which cause a decrease in efficiency are mainly a result of internal fluid flow back, called slippage.

Slippage is influenced by many factors and therefore those needs to be closely analyzed. Current models, on the one hand predict the trend of internal fluid loss, but on the other hand severely underestimate the amount of internal fluid loss.

Therefore it is essential to do new measurements, with a variety of operating conditions to design a new model to predict internal losses.

Measurements were performed at the Montanuniversitaet Leoben. The development of the new model should assist the calculation of slippage losses.

1.2. Pre - work

Previous this thesis pump tests were performed, which display the necessity of a new equation to calculate the slippage volume of Sucker Rod Pumps. These tests were performed as task of the Bachelor-thesis (*Systematic Comparison between the Standard Sucker Rod Pump and the SRABS – Pump*) [1] and are summarized in the SPE-192454-MS paper (*Volumetric Efficiency Evaluation of Sucker-Rod-Pumping Applications Performed on a Pump Testing Facility*) [2]. These tests were performed at the Pump Test Facility (PTF) at the Montanuniversitaet Leoben, under various operating conditions.
Results show that the current models in general confirm the trend of the measurements performed at the PTF, but severely underestimate the magnitude of internal loss. *"Measurements show that the losses per stroke are higher at least by the power of ten."* [2]
In conclusion of the SPE-Paper [2] additional tests shall be performed. More data-points need to be collected, therefore tests with various fluids, plunger types and different operating conditions should be performed. A significant amount of data points is necessary to develop a new general slippage model. With this model, it should be possible to predict losses for a variety of operating conditions.

2. Sucker Rod Pump

Hydrocarbon reservoirs are porous rocks, filled with pressurized liquid (oil, gas and water) buried in hundred to thousands meters of depth. The initial reservoir pressure before drilling and producing the reservoir is usually hydrostatic. In the beginning of the production stage, this pressure is sufficient to lift the fluid to the surface. This well-stage is called *natural flowing*.

Pressure losses in the petroleum production system (e.g. losses at restrictions, as a result of increased friction, change in fluid density, etc.) and the hydrostatic pressure in the well bore are counteracting the reservoir pressure. As long as the reservoir pressure is sufficient to overcome the sum of all the hindrances, the well will flow naturally. If this is not fulfilled anymore the well needs additional help to lift the fluid to the surface. According to [3] there are two main reasons why wells *die*:

- the well's flowing bottom hole pressure is less than the total pressure losses in the well; or

- the losses due to hindrances in the wellbore become higher than the required bottom hole flowing pressure needed to lift the fluid

To produce these wells it is then necessary to install artificial lift systems. One of the most common ways is the installation of subsurface pumps in the wellbore to pressurize the fluid and lift it to the surface.

The basic types of artificial lift systems are:

- Electric Submersible Pumps (ESP)

- Gas Lift

- Plunger Lift

- Processing Cavity Pumps (PCP)
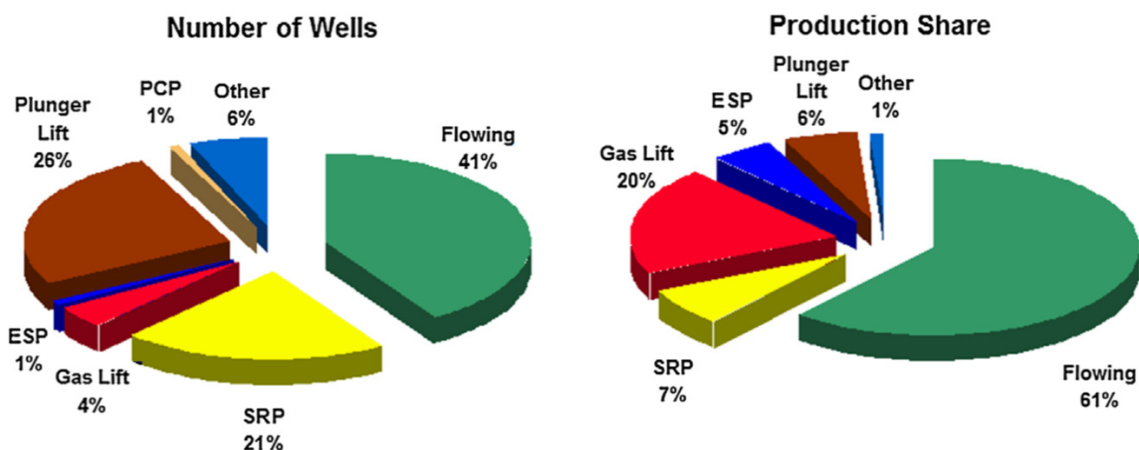
- Sucker Rod Pumps (SRP)

Figure 1: Artificial lift systems market share [3]

The most used artificial lift systems for onshore applications are Sucker Rod Pumps (SRP) and Electric Submersible Pumps (ESP), having a major share as illustrated in Figure (1). Furthermore, this graphic also illustrates the production share.

It can be seen that sucker rod pumps are installed in 21 percent of all wells but are only responsible for 7% of worlds total oil production.

According to [3] six percent of the total production share is given by plunger lift systems. In comparison to PCP, ESP and SR pumps plunger lift systems are used in gas wells for liquid removal. In most of the cases they are used for liquid removal in gas wells but have also already successfully been used in high-GLR oil wells. Another benefit of plunger lift systems is their prevention of paraffin precipitation and hydrate forming due to their scrapping action on the production tubing wall. Once installed in a clean and precipitation free tubing, the plunger constantly removes such formation deposits and therby reduces the necessity of methanol injection. The typical operating range for plunger lift systems is between 1,000 - 16,000 ft and liquid rates of 1 - 100 bbl per day. [4]

In comparison ESPs, which are installed in 1% of all oil-wells are responsible for 5% of total oil production. The following table clearly indicates, the lower production rates of Sucker Rod Pumps. This graphic also indicates that every artificial lift system has its specific working environment.

Artificial lift system	SRP	ESP	PCP	Gas lift
Max. operating depth, [ft]	16,000	15,000	12,000	18,000
Max. operating rate, [bpd]	6,000	60,000	6,000	50,000
Max. operating temp., [°F]	550	400	250	450
Fluid gravity, [API°]	>8	>10	<40	>15
Gas Handling	Fair to good	Fair	Good	Excellent

Table 1: Field of application [3] (modified)

Table 1 displays the application range of some artificial lift systems. It furthermore provides a decision aid, which system should be used for the given operating condition. SRPs have a high maximum operating depth, but the maximum produceable volume is limited by the material strength of the Sucker Rods [3]. ESPs in comparison are most of the time used for high rate wells.

The overall operating efficiency for Sucker rod pumps is slightly higher than for ESP. One of the major advantages of SRP is the flexibility and ability to change the production rate, in comparison with ESPs which have poor flexibility due to the almost fixed speed. Folling chapter will highlight the advantages and limitations of SRPs.

2.1. Advantages & Limitations

Sucker Rod Pumps are positive displacement pumps, therefore even a maladjusted pump will produce a certain amount of liquid to the surface. Their high reliability, ability to adapt to changing conditions and the run time efficiency provide an ideal system to produce mature reservoirs. Still, it is necessary to mention that as a result of their setup, sucker rod pumps are limited by the operating depth. [3]

At high depths, the limiting factor is most of the time the rod string. High cyclic loads, which act on the long rod string, lead to high elongation and contraction forces resulting in early fatigue. However, well-engineered SRP are applicable for deep wells.

According to [3] the main advantages and disadvantages of Sucker Rod Pumps are:

+ Pumping capacity could be adjusted easily

+ Simple to design and operate

+ High reliability and run time efficiency

+ Fast maintenance due to high replacement-parts availability

+ Supply and availability of repair parts is fast and constantly given

− Poor gas handling capacity

− Depth limitations by the mechanical strength of the rod

− High frictional wear in deviated wells

− Sand production has a severe negative impact on the life of the pump

Usually the rod strength is the limiting factor of SRPs. The design of the rod string is based on different influencing factors e.g. production rate, tubing size, environmental conditions and the setting depth.

2.2. Components

Sucker Rod Pumps (SRP), Walking Beam Pumps or Rod Pumps in general consist of a surface and sub-surface unit.

Figure 2: Schematic of a Sucker Rod Pump [5]
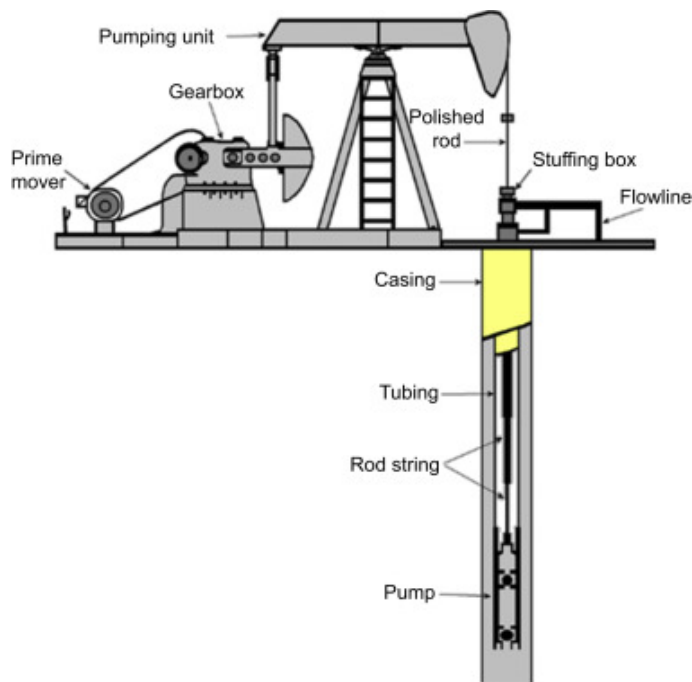
As illustrated in Figure 2 the prime mover is connected to the gearbox via a v-belt and on the other side to the crankshaft. The arrangement of horsehead, walking beam, pitman and crank convert the rotary movement of the primemover to a reciprocating up- and downward movement of the rod string. The rod string connects both, surface and subsurface components of the system.

The subsurface pump consists of moving and non-moving parts. It could therefore be separated into two major components:

1. The **Barrel**, which is usually the non-moving part of the pump is fixed onto the tubing and acts as housing for the moving plunger. The standing valve is connected to the bottom of the barrel, acting as the intake valve, allowing the fluid to enter the pump.

2. The **Plunger** is the moving part of the pump. It is connected to the sucker rod string at its top. The traveling valve is fixed at the bottom of the plunger, acting as the outtake valve of the pump.

The moving part of the pump, the plunger, is closely fitted to barrel. The distance between plunger and barrel is called clearance and should be kept as small as possible to avoid uncontrolled fluid passage. The clearance is normally in the range of a few thousands of an inch, but still it is necessary to allow a little amount of fluid slip to maintain proper lubrication of the metal to metal interface. Clearance should also be adapted to the sand particle size. The clearance should be either large enough to let the sand particles pass without further damage of the interface or small enough that sand particles are not able to enter the gap between plunger and barrel.[6].

According to [4] *tight clearances* are less than 0.003 inches and *loose clearances* are greater than 0.008 inches.

Further specifications can be found in API SPECIFICATION 11AX [7]

The combination of the two ball valves (standing and traveling valve) and their alternating opening and closing, results in the pumping operation. Most of the fluid is pumped during the upstroke.

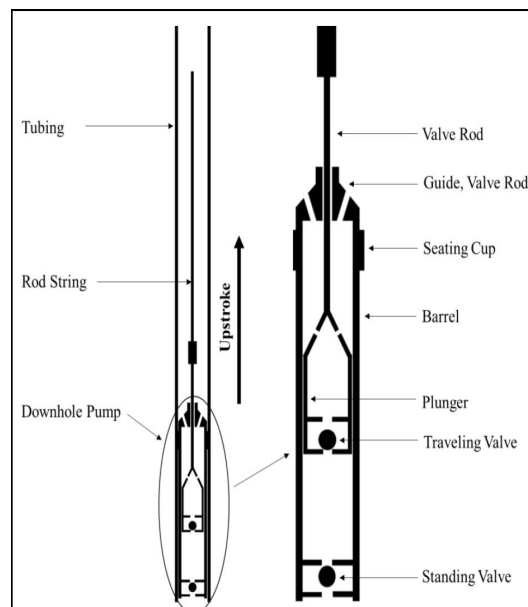Figure 3: Schematic of a standard Sucker Rod Pump [2]

Figure (3) pictures the working principle of a SRP. During the upstroke, visualized by the upward-pointing arrow, the traveling valve is closed. The plunger starts to travel upward at the bottom of the pump, close to the standing valve (bottom dead center). The surface unit lifts the rod, the plunger and the fluid. During the upstroke the standing valve gets

opened by the reservoir pressure, allowing fluid to enter the pump. At the deflection point (top dead center) the plunger starts to travel downward. Shortly after the downstroke began, the traveling valve opens and the standing valve closes. During the downstroke the plunger gets filled with fluid, but also displaces fluid. The amount of displaced fluid on the downstroke, is equal to the volume of the plunger itself and results in a downstroke production. At the bottom deflection point (bottom dead center) the loop starts again.

2.3. Design

Every artificial lift system is designed to produce fluid in an economic and efficient way. This thesis has a special focus on the downhole pump.

2.3.1. Plunger and pump design

Specification and Designation according to API SPECIFICATION 11AX [7]:

   a. Nominal tubing size

   b. Basic bore diameter

   c. Type of pump, including type of the barrel and location and type of seating assembly

   d. Barrel length

   e. Plunger length

   f. Length of each extension when used

These pump geometries are essential for designing a sucker rod pump. Furthermore, the type of barrel, plunger and the type of seating assembly is essential. Besides the design of the main parameters, the design also includes a proper material selection in order to counteract harsh environmental downhole conditions [3].

To proper design a downhole pump, the operator also needs to be aware of the resulting forces which act during operation. The operators' goal is to be as efficient as possible and this lies in the proper design of the pumping mode. The pumping mode is a function of acting loads, pumping speed, stroke length, plunger size and rod string design [3].

The American Petroleum Institute (API) defined standards for the pumping mode. Nowadays also software helps to proper design a pump. Many combinations of pumping speed, pump size and stroke length are available. Which does not mean that every combination is applicable for one specific pump.

The API published a recommended procedure (*API RP 11L*) to calculate the pump mode. Also pre-calculated schemes are available to fit the design to a certain volume rate. Nevertheless, it is not always possible to design a pump with a pre-defined scheme. Recommended practices (RP) are based on investigations of certain pumping modes but still assume certain conditions. RP describes a general way to design a pump to achieve the highest flow rate as possible.

XX - XXX X X X X   X - X - X - X

Tubing size: 15 [1.900 in. (48.3 mm) OD]
20 [2³/₈ in. (60.3 mm) OD]
25 [2⁷/₈ in. (73.0 mm) OD]
30 [3¹/₂ in. (88.9 mm) OD]
40 [4¹/₂ in. (114.3 mm) OD]

Pump bore (basic):   125 [1¹/₄ in. (31.8 mm)]
150 [1¹/₂ in. (38.1 mm)]
175 [1³/₄ in. (44.5 mm)]
178 [1²⁵/₃₂ in. (45.2 mm)]
200 [2 in. (50.8 mm)]
225 [2¹/₄ in. (57.2 mm)]
250 [2¹/₂ in. (63.5 mm)]
275 [2³/₄ in. (69.9 mm)]
375 [3³/₄ in. (95.3 mm)]

Type pump: R (rod)
T (tubing)

Type barrel: H (heavy wall for metal plunger pumps)
W (thin wall for metal plunger pumps)
P (heavy wall for soft-packed plunger pumps)
S (thin wall for soft-packed plunger pumps)
X (heavy wall for metal plunger pumps, thin
wall thread configuration)

Location of seating assembly: A (top)
B (bottom)
T (bottom, traveling barrel)

Type seating assembly: C (cup)
M (mechanical)

Barrel length in feet

Nominal plunger length in feet

Length of upper extension in whole feet

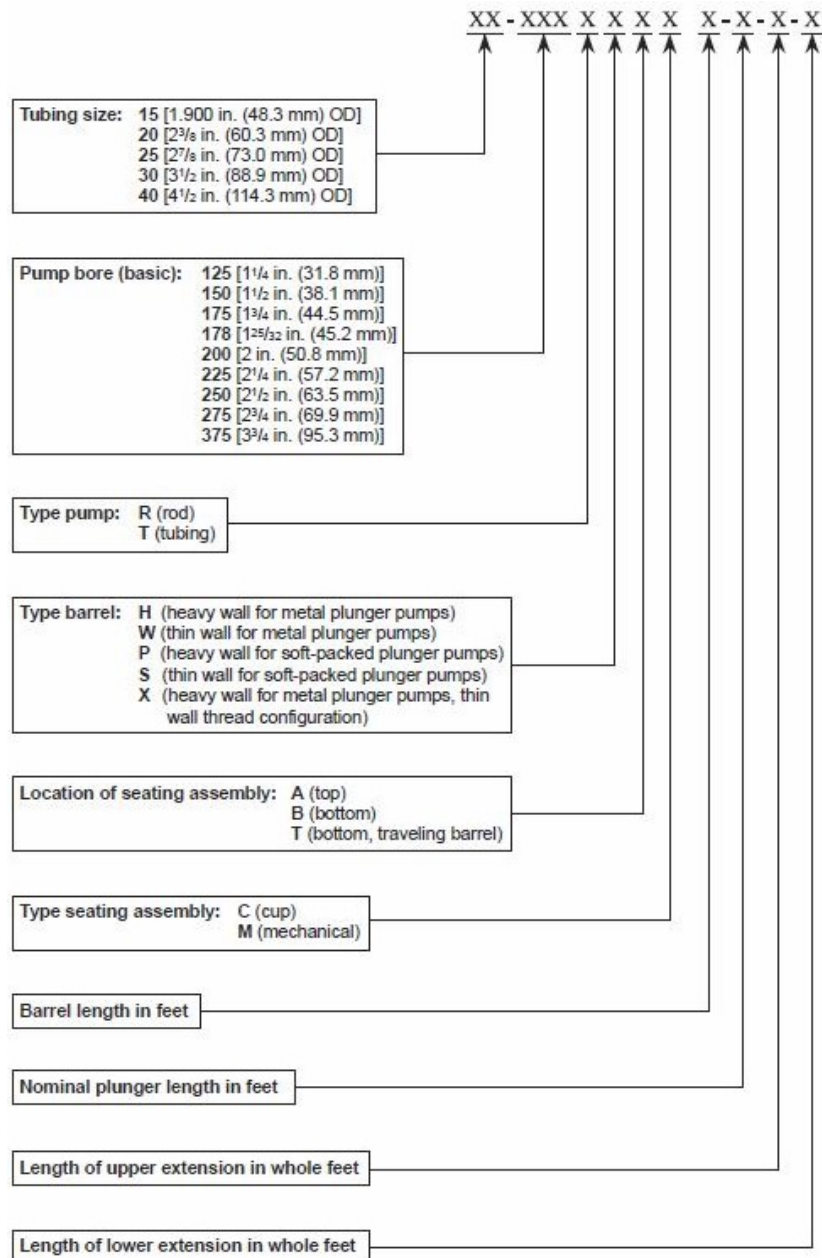Length of lower extension in whole feet

Figure 4: Pump designation [7]

Figure (4) illustrates the pump designation and design possibilities of down hole sucker rod pumps.

2.4. Fluid loss

This chapter will focus on the efficiency of sucker rod pumps and will have a close look on fluid losses. Fluid- or particle erosion and the presence of a sour environment have a severe impact on the efficiency of sucker rod pumps. These parameters effect the sealing efficiency of valves and influence the interface between plunger and barrel.

All calculations in this thesis assume a full pump. A full pump means that the plunger is completely filled with liquid at the beginning of the upstroke. As sucker rod pumps are designed for single-phase production also gas will be excluded. Nevertheless the presence of gas has a severe impact on the efficiency of sucker rod pumps which will be explained in the following Chapter 2.4.1.

2.4.1. Gas - interference

In the presence of gas the volumetric efficiency decreases drastically. Worst case of this scenario is when the pump is so called *gas locked*. In this case their is almost only gas in the pump, which gets compressed and de-compressed during down- and up-stroke and no fluid is pumped anymore [8].

Therefore, the presence of gas has a direct impact on the volumetric efficiency. One further needs to distinguish between *free gas* and *gas in solution*. The presence of free gas influences the type of completion. In 1963 Clegg [8] published a paper which describes the challenges of gas during artificial oil production. To combat the gas interference he proposed to analyze the pumping conditions as depicted in the following graphic:

Figure 5: Pump efficiency in the presence of gas [8] (modified)

To describe the efficiency of SRPs, as depicted in Figure 5 he assumed that there is no clearance between plunger and barrel and therefore no slippage and furthermore that there is no space between traveling and standing valve at the bottom of the stroke.

If the pump intake pressure is higher than the bubble point pressure all gas stays in solution and the presence of gas has hardly any impact on the efficiency variation of the pump. The curve from B to F describes the presence of free gas (pump intake pressure is below bubble point pressure) and a sharp decrease in pump efficiency. In this case all gas is pumped and in the worst case this would lead to a *gas-lock*. The pump is called to be gas locked if the pressure above the traveling valve is higher than the pressure below. In this case the fluid below is just gas, which gets compressed. If the bottom dead center is reached during the downstroke and the pressure of the compressed gas inside the barrel is lower than the pressure above the traveling valve, the traveling valve does not open and no fluid enters the plunger. Proper compression is essential to avoid this state. This can be achieved if the pump spacing is well designed and the distance between traveling valve and standing valve is small at the bottom of the stroke.

To increase efficiency again the installation of a gas-anchor is mandatory. According to [8] the separation efficiency between gas and oil is linked to the bubble size of the gas. Bigger bubbles, present when the pressure is reduced, allow faster and better separation.

A well designed pump setting depth and gas anchor, therefore results again in a highly efficient pump.

To summarize the Figure 5, the setting depth of the pump should be deep enough to ensure that the intake pressure is higher than the bubble point pressure or as shallow as possible to ensure large gas bubbles for efficient separation.

In general, if gas is present, the installation of a gas separation tool is recommended. Most of these tools work with the principal of gravitational separation. Since gas has a lower density than oil it will rise faster. Most of the systems are designed with a down-flow of oil before intake and a vent of gas at the top of the tool. Lowering the intake pressure increases the bubble size and the separation efficiency. The best efficiency can be achieved, if the gas is completely vented before entering the pump. Efficiencies up to 100% can be reached.

If the pump intake pressure is above the bubble point pressure, 100 % pump efficiency can not be reached. The gas is still in solution, which results in a higher oil volume under down hole conditions compared to stock tank conditions where the gas is not in solution anymore.

Besides the installation of a gas separation tool e.g. a *natural, packer-type* or a *poor-boy* a well designed pump is essential. In the presence of gas, proper pump spacing and a high compression ratio is required to ensure production. Clegg also recommends a smaller cage design for the ball valves. Since those space reduces the stroke length and therefore minders the compression ratio. [8]

Besides that different types of sucker rod pumps exist, which should be taken into account in the presence of gas e.g. the *gas-breaker pump* or the *Panacea pump*. [3]

2.4.2. Theoretical produceable volume

The maximum produceable volume per stroke is only a function of geometry.

$$Q_{max} = \frac{d_p^2 \pi}{4} h_{eff} \tag{1}$$

Q_{max} is the maximum produceable volume, of liquid in [m^3], d_p is the plunger diameter in [m] and h_{eff} is the effective stroke length at the plunger [m]. Q_{max} is therefore a product of plunger-area times the effective stroke length.

Equation 1 describes the theoretical volume, which a pump is able to produce per one stroke. h_{eff} can not be directly transferred to the polished rod stroke length. In between polished rod and plunger is the sucker rod string. The elastic behavior of the sucker rod string in combination with cyclic loads applied on the rod, result in rod stretch and contraction. To derive the effective stroke length of the plunger, the damped wave equation needs to be solved. Therefore, appropriate boundary and initial conditions need to be selected.

The solution of the wave equation describes the displacement of a pre-selected point in time and furthermore displays the load on the string. These loads can be visualized as surface- and downhole-pump-card, which furthermore gives information of the pump condition. [9]
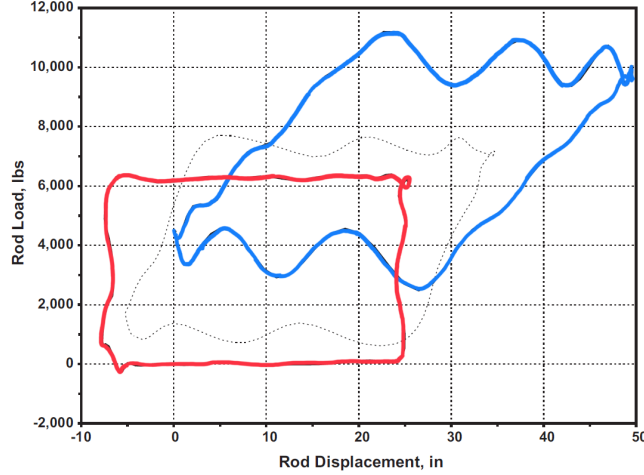
Figure 6: Example of a calculated downhole card and a surface card (modified) [3]

In addition the solution of the damped wave equation also gives information about the downhole pump condition. Figure 6 displays the polished rod load of the Sucker Rod Pump which is measured on the surface (blue curve). This polished rod surface card is then converted to the downhole card (red curve), with the help of the damped wave equation. The shape of the downhole card is a useful tool to investigate the pumps condition. Malfunctions e.g leaking valves, gas presence, pump off condition, etc. can be easily depicted from a well derived downhole card.

2.4.3. Volumetric efficiency

The parameter *volumetric efficiency* describes the ratio of actual produced volume to theoretical produceable volume. The difference between these two volumes is the sum of all fluid losses, which include losses at the valve and at the barrel - plunger interface.

$$\eta = \frac{Q_{actual}}{Q_{theoretical}} \tag{2}$$

Q_{actual} is the actual produced volume of liquid in [m^3] per stroke, $Q_{theoretical}$ is the maximum produceable volume of liquid in [m^3] per stroke.

The barrel - plunger interface creates a metal to metal seal. This interface is effected by environmental conditions e.g. sour components in the fluid, or the presence of fines. The distance between the nominal outside diameter of the plunger and the nominal inside diameter of the barrel is called clearance. This clearance is affected by several circumstances and could increase during the lifetime of the plunger. The surface of the plunger and the barrel will be rubbed off, in the presence of sand, leading to an increase in clearance and therefore, a decrease in volumetric efficiency. According to [7] this distance is in the range of a few hundredths of millimeters (thousandths of inches).

2.4.4. Slippage

Fluid, which slips back through this clearance, is called slippage volume. A certain amount of slippage is required to lubricate the metal to metal seal of plunger and barrel, to avoid high friction and plunger sticking. Furthermore, in the presence of fines it is necessary to allow these particles to slip through the clearance without surface destruction.

If the clearance is designed to small, fines could add additional friction between plunger and barrel and therefore cause plunger sticking. Plunger sticking results in additional compressive loads on the rod string, minimizing the lifetime of the whole system [3].

2.4.5. Fluid loss due to valve overlap

In common sucker rod pumps, ball valves are used. Proper functioning of the SRP depends on a proper function of the ball and seat assembly. The integrity of this assembly is mostly influenced by the operating conditions. Valve failures, in general, are a result of the presence of fines, fluid composition and improper material selection.

To ensure proper sealing following steps should be taken into account:

1. In the presence of sand, the installation of a sand-screen should be taken into account. This restricts the amount of sand entering the pump. The use of sand-screens minimizes the risk of abrasion and clogging of surface and downhole equipment. [3]

2. Improper material selection could lead to early valve failure. The presence of a sour environment in combination with or without abrasive materials should influence the material selection. Table 2 illustrates the recommended materials according to [7]

3. The pump setting depth gathers the pressure gradient across the ball-seat assembly. A high-pressure gradient and therefore high velocity at the valve, plus the presence of abrasive material promote the erosion and therefore prevent perfect sealing of the valves.

Symbol	Description	Hardness	Material
A1	Stainless Steel	Ball: HRC 58-65.0 Seat: HRC 52.0-56	UNS 41000-UNS 44000
B1	Cobalt Alloy, Cast	Ball: HRC 56.0-63 Seat: HRC 50-65.0	Cobalt, chromium and tungsten alloy
B2	Cobalt Alloy, Powder Metal	Ball: HRC 53.0-60 Seat: HRC 51-57.0	Cobalt, chromium and tungsten alloy
C1	Tungsten Carbide	Ball: HRA 88.0-89 Seat: HRA 88-89.5	Tungsten with Cobalt binder
C2	Nickel Carbide	Ball: HRA 89.0-90 Seat: HRA 87.5-89	Tungsten with Nickel binder
C3	Titanium Carbide	Ball: HRA 89-90.5 Seat: HRA 89-90.5	Tungsten and titanium carbide with cobalt binder

Table 2: Ball and seat material [7] (modified)

The abbreviations *HRA* and *HRC* describe types of hardness measurements. *HR* describes the hardness according to *Rockwell*, where *A* and *C* are specific scales. *A* and *C* describe the load and shape of the indenter which is a hardened steel ball for *A* and a diamond cone for *C*. The Rockwell hardness measurement is a fast and reliable hardness measurement, with relative low measurement time. [10]

Table 2 displays material hardness between 52 and 90. It furthermore displays different materials with different chemical and physical properties. For example, Nickel Carbides have a high H_2S and CO_2 resistance, Chrome plated Barrels are used in a severe abrasive environment and Cobalt-Alloys which have a high wear and corrosion resistance. In general, all Carbide-alloys have a high hardness.[11].

Another influencing factor of the volumetric efficiency is the opening and closing duration of the ball valves. Previous this thesis (Chapter 1.2) measurements with two different valve types were performed, illustrating a difference in opening and closing time. The two pumps namely the SRP and the Sucker Rod Anti Buckling System Pump (SRABS) differ in the way of their assembly, valve positioning and valve assembly. The SRP is equipped with normal ball valves whereas the SRABS-pump has a cylindrical, heavier ring valve which is illustrated in Figure 7.
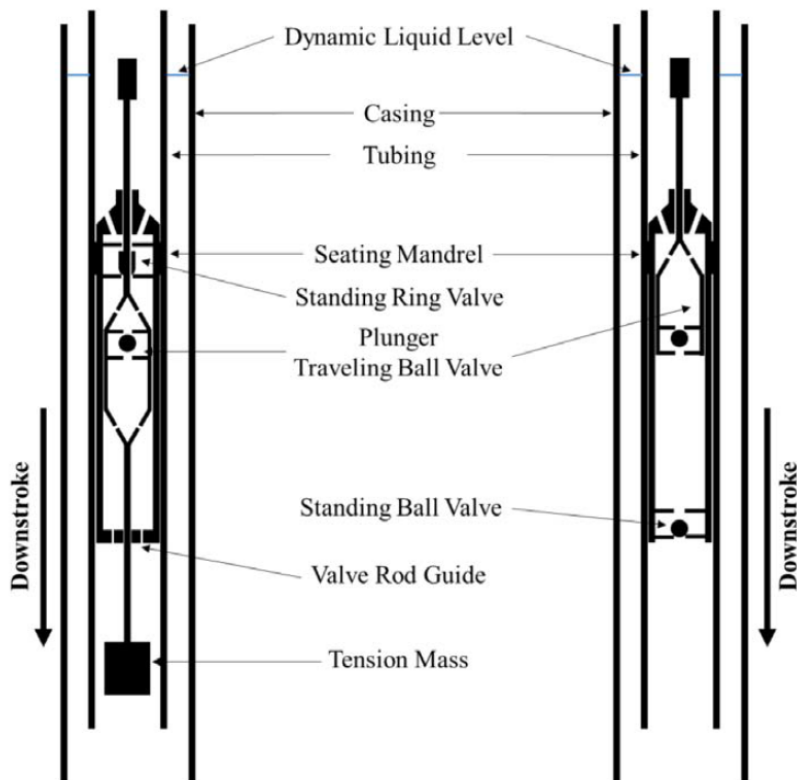
Figure 7: Comparison between SRABS pump and a conventional SRP [12]

Figure 7 furthermore illustrates the assembly of the Sucker Rod Anti Buckling System (SRABS) Pump on the left side and on the right side a conventional sucker rod pump is depicted. The biggest advantage of the SRABS pump compared to a standard SRP pump is the buckling reduction of the sucker rod during during the downstroke of the pump. This is achieved by an additional tension mass at the lower end of the pump.

Most of the time buckling is tried to be reduce by the use of heavy sinker bars at the lower end of the sucker rod string. A major disadvantage of sinker bars is their additional weight on the sucker rod string which could lead to higher lifting costs. When using the SRABS-system the number of heavy weight sinker bars can be reduced significantly, which results is an overall higher pumping efficiency and higher pumping speeds. [12]

(a) Valveoverlap SRP   (b) Valveoverlap SRABS
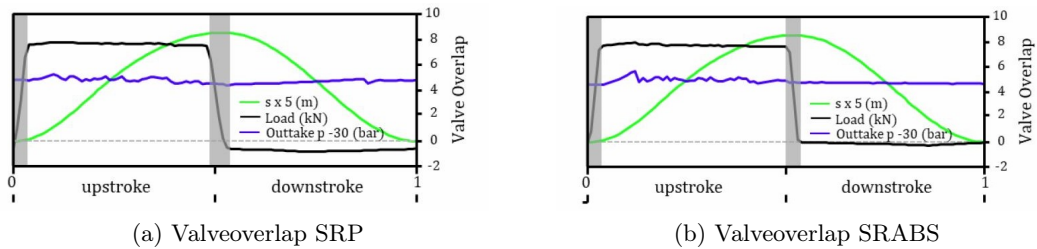
Figure 8: Valve overlap of different pump types [2]

The previous measurements show a delayed closing of the SRP valve compared to the SRABS valve. For a speed of 1 Stroke Per Minute (SPM) the SRP valves requires 3 second to close and open, which is equivalent to a travel distance of 3cm for the pump plunger. Nearly the same distance was measured for higher pumping speeds. By contrast with, the SRABS only needs 1.8 s or a distance of 0.025 cm of plunger travel to close. During this period fluid is able to flow back through the valve, resulting in a decrease of efficiency. [2]

The valve overlap is illustrated by Figure 8. The left side illustrates the overlap of the standard SRP, the right side illustrates the overlap of the SRABS pump.

3. Historic Slippage models and Slippage model derivation

The following chapter describes the fluid mechanical behavior of slippage, the derivation of the basic slippage model and a comparison between actual models. The proper formulation of an accurate model is necessary for rod pump operators. Improper designed pumps are inefficient, cause high costs and may fail earlier due to higher wear.

3.1. Rheological-model

Following chapter is generated with information from [13], [14] and [15].

Rheological models are necessary to describe fluid behavior and fluids viscosity. In general, fluids can be divided into two groups. *Newtonian* fluids describe a linear relation between shearing stress and shearing strain. Fluids which do not have a linear relation, are normally referred to *non-Newtonian* fluids.

Generally there are three important models, namely the Newtonian model, the Bingham-plastic model and the Power-Law model.

Newtonian models approximate fluids like water, gas and high gravity oils. Nevertheless fluids can not always be described by the Newtonian model.

For example, most of the fluids used in drilling operations e.g. slurry and cement are to complex to be described by a simple linear relation like the Newtonian model. A direct proportionality between shear stress and shear rate is not given, more advanced models are needed to describe certain fluid behavior.

3.1.1. Newtonian model

Following chapter is based on [14]. The simplest model to describe a fluid is the Newtonian model. It states that the shear stress is direct proportional to the shear rate:

$$\tau = \mu\dot{\gamma} \tag{3}$$

where μ is the constant of proportionality of the fluid, τ is the shear stress which is applied on the fluid and $\dot{\gamma}$ is the shear rate. The slope is also often referred to the apparent viscosity. It is necessary to mention that the apparent viscosity for Newtonian fluids is the same as the actual viscosity and it is therefore independent of the applied shear rate.

This concept is based on a theoretical model where a solid surface is in contact with a liquid surface while the solid is pulled with a constant force. This pulling results in a stress on the liquid which is acting in the opposite direction, displayed by Figure 9. At equilibrium conditions on could state that: $P = \tau * A$ where A is the effective Area in contact with the fluid, τ the shearing stress and P the pulling force. As a result of the applied force the plate will move with constant velocity. The upper part of the fluid will move with the same velocity as the plate itself, due to the no-slip condition. This results in a fluid deformation displayed by the points B and B' [14].
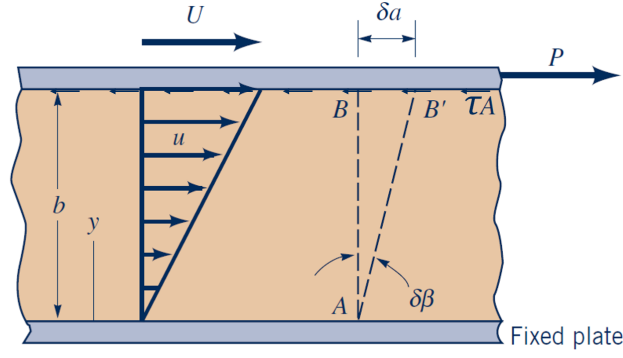
Figure 9: Material deformation between two plates (modified) [14]

The velocity of the fluid is a function of the distance between the two surfaces in which the fluid is. Fluid velocity is: $u = u(y)$ which increases form bottom $u = 0$ to top $u = U$ where U is the plate velocity. The change in velocity with distance between the two plates is linearly and according to [14]:

$$\dot{\gamma} = \frac{du}{dy} = \frac{U}{b} \tag{4}$$

$\dot{\gamma}$ is called the shear rate or shearing rate, which is a result of the upper plates velocity and the distance between those two plates. The concept of shearing rate is later used to match the corresponding viscosity to its shearing rate.
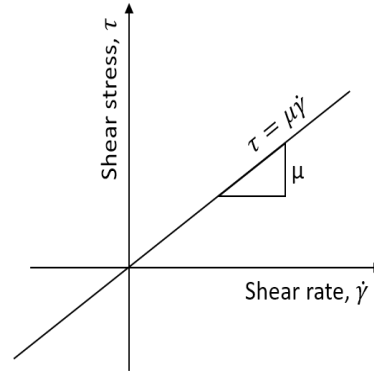
Figure 10: Newtonian fluid model [13]

Figure 10 displays the Newtonian behavior of a fluid. It displays the linear relationship between shear stress and shear rate. The best example for a Newtonian fluid is water.

3.1.2. Power-Law model

The Power-Law model is used to describe more complex fluids, where the relation between shear stress and shear rate is not a linear, according to [13].

$$\tau = K\mu * |\dot{\gamma}|^{n-1}\dot{\gamma} \tag{5}$$

This model requires two parameters to characterize a fluid. The parameter n describes the degree of non-Newtonian behavior of a fluid. With $n < 1$ the fluid behaves pseudoplastic, with $n > 1$ the fluid behaves dilatant and with $n = 1$ the fluid behaves Newtonian. K describes the consistency index.

Fluids with $n < 1$ are also called *shear thinning* fluids, since their viscosity decreases with increasing shear rate. This means, the harder the fluid is sheared the less its viscosity becomes. Fluids with $n > 1$ are also called *shear thickening* fluids, since their viscosity increases with increasing shear rate. The parameter K describes the consistency index of the fluid. *Pseudoplastic* fluids are characterized by a decrease in viscosity with an increase in shear rate. *Dilatant* fluids are characterized by an increase in viscosity with an increase in shear stress.

Figure 11 and Figure 12 display the Power-Law model with respect to the flow behavior index n.
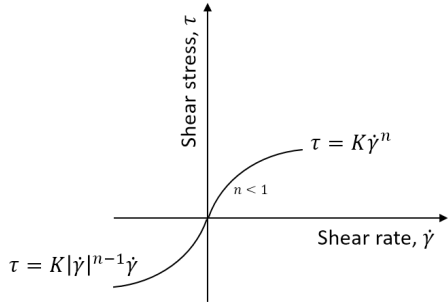
Figure 11: Pseudoplastic
Power-Law [13]
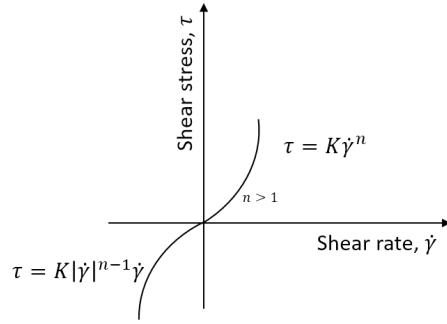
Figure 12: Dilatant
Power-Law [13]

Fluids with a certain offset at the y-axis for zero shear rate can be described according to [16] as (also called: Herschel-Buckley fluid):

$$\tau = \tau_0 + K * \gamma^n \tag{6}$$

3.1.3. Rotational viscometer

Rotationals viscometer are used to measure the viscosity of a fluid, while using a rotating sleeve around a concentric cylinder compared to the theoretical approach of relative movement of parallel plates. The rotator-sleeve is rotating at a constant speed while the bob is held motionless. The applied torque on the bob is a result of the fluids viscous drag acting on the bob, generated by the rotating sleeve. The torque which acts on the bob must be equal and opposite in direction to the torque applied by the motor to the rotor [13]. Figure 13 displays the bottom view of a rotational viscometer.
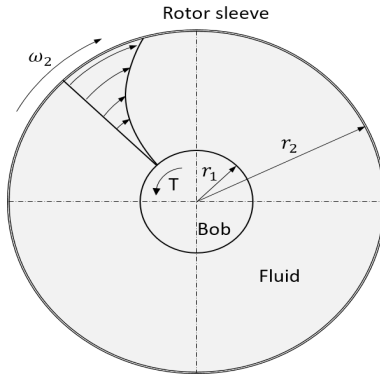
Figure 13: Rotational viscometer [13]

The rotation of the bob relative to its initial position can be then read from the dial. With the dial reading and its related and pre-set motor speed, the viscosity of the fluid can be calculated by using adequate models. The rotating speed is varied and increased, which results in an faster rotation of the bob. The variation of the rotor speed and its corresponding bob angle needs to be noted and then converted with an appropriate model.

According to [15] one of the models, used to calculate viscosity, is the following:

$$\tau = k_1 k_2 \theta \tag{7}$$

$$\dot{\gamma} = k_3 N \tag{8}$$

$$\mu = \frac{\tau}{\dot{\gamma}} 100 \tag{9}$$

Where k_1 is the torsion spring constant, k_2 is the shear stress constant for effective bob surface $[cm^{-3}]$ and k_3 is the shear rate constant $[sec^{-1} \ per \ rpm]$. Each viscometer and model requires specific constants, which are normally defined in the instruction manual.

This model is used to calculate the viscosities for the used fluids in this thesis.

3.1.4. Xanthan Gum

This chapter briefly describes the kind of used viscousifying agent and its chemical structure and usage. The main references of this chapter are [17] and [18]. Besides the food industry Xanthan Gum is also used as a part of tertiary oil recovery. The bio-polymer Xanthan Gum D (or S-ES BIO XG) is a polysaccharide. Polysaccharides in general are carbo-hydrates which are build out of many mono-saccharides. For example starch or cellulose.

Carbonhydrates

Xanthan gum is a polysaccharide but there are also different kinds of saccharides:

1. Monosaccharide

2. Oligosaccharide

3. Polysaccharide

Those three different saccharide describe the main classification of carbohydrates. Most of these compounds have a base structure like $C_x(H_2O)_y$.

Monosaccharides for example have a chain length of two to six carbon-atoms. In addition to this chain monosacchrides have either an aldehyde- or a ketone-group bonded to their structure. Monosaccharides are also called *simple sugar* and represent the most basic form of a saccharide.

The combination of two monosacchrides (do not have to be the same) results in a disaccharide which is also called Oligosaccharides. Oligosaccharides are the result of the loss of a H_2O molecule and the formation of a ether-group.

Polyssacharides $(C_6H_{10}O_5)_x$ are made of $_D$-Glucose molecules. The result of the fermentation process of *Xanthomonas campestris* in the presence of a carbo-hydrate substrate and other grow supporting nutrients is Xanthan Gum, the used polysaccharide for the experiments. [18] Due to this fermentation process Xanthan Gum forms to protect the bacterial cells. This protective property is the main cause why Xanthan is so stable compared to other polysaccharides.

According to [18] Xanthan Gum shows high tolerances under several conditions. It is still stable under a wide pH range (1-13), a high concentration of salt and under boiling temperatures. For the experiments in the lab fresh water was used at ambient temperature. Therefore the operating conditions should not effect the chemical structure.
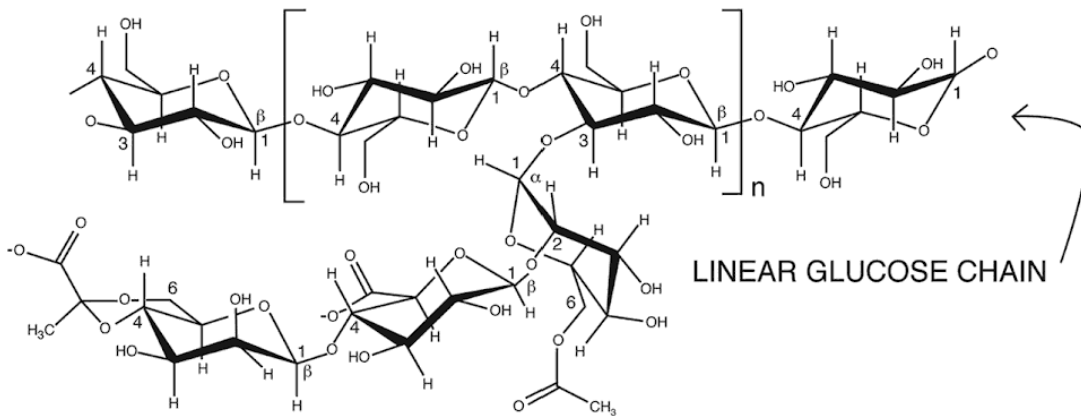
Figure 14: Structure of Xanthan Gum [18]

Figure 14 displays the structure of Xanthan Gum. The figure indicates a three dimensional molecule structure.

During the preparation of the modified fluids it was recognized that the polysaccharide formed clumps. According to [18] this behavior is normal for cold water mixtures and can reduced with appropriate agitation. Therefore the modified fluids were appropriately stirred and the mixture was pumped in cycles to the facility previous the measurements to ensure homogeneity.

The stability of Xanthan Gum maybe good for short term operations, but between the measurements a change of the fluid was recognized. The mixture was stored in a tank at the bottom of the facility. This tank is used as a reservoir providing the intake pump with fluid to simulate the reservoir pressure. This tank is open to the environment.

Between the measurements a certain amount (about 2-4 days) of time passed by. After such a long time a separation of the mixture was recognized resulting in a decomposition of the Xanthan Gum water mixture. The base of the tank was occupied with a higher viscous fluid than the top of the tank. A remixuring of the fluid was not possible anymore and therefore the fluid needed to be changed. This resulted in the use of many different modified fluids with different viscosities, which has a positive side effect on the range of the established model.

3.2. Slippage model

Main references for this chapter are [19], [6] and [14].

Since slippage is fluid loss in the annulus of the stationary barrel and the moving or non-moving plunger (both cylindricaly shaped), slippage can be interpreted as flow between two circular tubes.

Slippage in general is described by the solution of the Navier-Stokes equations.

3.2.1. Navier-Stokes

To describe flow between the annulus of two bodies, it is necessary to solve the Navier-Stokes equations for the specific problems and their associated boundary conditions.

Navier-Stokes in vector notation (for Newtonian and incompressible fluids:) [14]:

$$\rho\left(\frac{\partial \mathbf{V}}{\partial t} + \mathbf{V} \cdot \nabla \mathbf{V}\right) = -\nabla p + \rho g + \mu \nabla^2 \mathbf{V} \tag{10}$$

Where V describes the velocity vector, ∇ describes the vector differential operator, which calculates the change in velocity in each direction. ∇p describes the pressure gradient between two points, ρg describes the gravitational acceleration and ∇^2 of V describes the second derivative of the velocity vector at a specific point. Furthermore it can be seen that the left part of the equation describes the acceleration of the fluid and the right part the forces acting on the fluid. The Navier-Stokes equation is the general base equation to describe incompressible Newtonian fluid flow. However, because of the complexity of the Navier Stokes equation, no known analytical solution of the Navier-Stokes is present [14]. Most of the fluid flow problems are described either empirically or as a numeric solution of Equation 10.

Navier-Stokes equations and simplifications

To simplify the solution of the Navier-Stokes equation assumptions were made.

The property of compressibility for fluids can be described with the bulk modulus. The compressibility of water and mixtures of water and Xanthan-Gum is assumed to be zero. Since fluids in general have large bulk-modi, fluids a relatively incompressible. Therefore there is no volume or density change assumed, if pressure is applied. Additionally, the amount of gas dissolved in the fluid is assumed to be zero. [14]

Further assumptions are:

- Constant viscosity

- Two-dimensionality: components in z-direction equal to 0

- Steady state $\partial \mathbf{V}/\partial t = 0$

- Fully developed laminar flow $\partial/\partial x = 0$

- No-slip condition

- Newtonian and incompressible fluid

- No dissolved gas in the fluid

With the help of the conservation of mass for a fully developed two dimensional flow we know that $\partial v / \partial y = 0$:

$$\underbrace{\cancel{\frac{\partial u}{\partial x}}}_{\text{fully developed}} + \frac{\partial v}{\partial y} + \overbrace{\cancel{\frac{\partial w}{\partial z}}}^{\text{two-dimensionality}} = 0 \tag{11}$$

Furhtermore we know, or assume, that there is no velocity in y or z direction and therefore: $v = 0$ and $w = 0$. We set $g_x = 0$ because we assume that there is no gravitational force acting in the x-direction. According to [14] the Navier-Stokes equations for rectangular coordinates are:

Momentum in x-direction

$$\rho\bigg(\underbrace{\cancel{\frac{\partial u}{\partial t}}}_{\text{steady state}} + u\overbrace{\cancel{\frac{\partial u}{\partial x}}}^{\text{fully developed}} + v\overbrace{\cancel{\frac{\partial u}{\partial y}}}^{\text{two-dimensionality}} + w\,\cancel{\frac{\partial u}{\partial z}}\bigg) = -\frac{\partial p}{\partial x} + \rho\cancel{g_x} + \mu\bigg(\underbrace{\cancel{\frac{\partial^2 u}{\partial x^2}}}_{\text{fully developed}} + \frac{\partial^2 u}{\partial y^2} + \overbrace{\cancel{\frac{\partial^2 u}{\partial z^2}}}^{\text{two-dimensionality}}\bigg) \tag{12}$$

Momentum in y-direction

$$\rho\bigg(\underbrace{\cancel{\frac{\partial v}{\partial t}}}_{\text{steady state}} + u\overbrace{\cancel{\frac{\partial v}{\partial x}}}^{\text{fully developed}} + v\overbrace{\cancel{\frac{\partial v}{\partial y}}}^{\text{two-dimensionality}} + w\,\cancel{\frac{\partial v}{\partial z}}\bigg) = -\frac{\partial p}{\partial y} + \rho g_y + \mu\bigg(\underbrace{\cancel{\frac{\partial^2 v}{\partial x^2}}}_{\text{fully developed}} + \cancel{\frac{\partial^2 v}{\partial y^2}} + \overbrace{\cancel{\frac{\partial^2 v}{\partial z^2}}}^{\text{two-dimensionality}}\bigg) \tag{13}$$

Momentum in z-direction is zero due to the two-dimensionality.

After the simplification of the Navier-Stokes equations we now know that the Momentum in y-direction describes the hydrostatic pressure. The momentum in x-direction states:

$$0 = -\frac{\partial p}{\partial x} + \mu\bigg(\frac{\partial^2 u}{\partial y^2}\bigg) \tag{14}$$

With the help of the conservation of mass equation, in combination with the three Navier-Stokes equations above it is possible to mathematically describe the fluid flow of an incompressible newtonian fluid. Nevertheless, only a few problems are possible to describe by solving the Navier-Stokes equations analytically. Approximated solutions and numerical approaches provide in many cases an adequate approach to solve certain fluid flow behaviors. [14]

3.2.2. Flow between two non-moving plates (Navier-Stokes)

In general, the fluid flow between barrel and plunger can be described as the fluid flow between to cylindrical elements Figure 15 (Navier-Stokes in terms of cylindrical polar coordinates). As shown in Figure 15 the plunger is moving and is therefore affecting the parabolic velocity profile. The velocity on the barrel surface is zero, due to the no-slip condition the velocity of the fluid at the plunger is the same as the plunger velocity. The maximum is not in the middle anymore (as in Figure 16) but shifted towards the moving plunger.
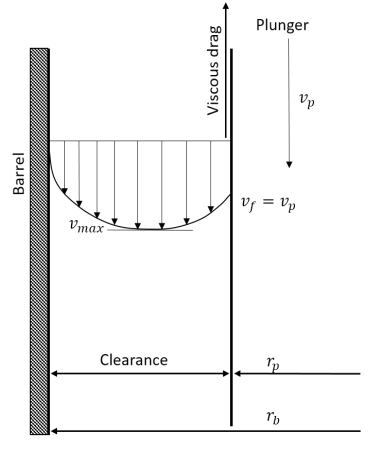
Figure 15: Fluid velocity profile, downward moving plunger

However, if the distance between these two elements is rather small, fluid flow can be also described as flow between two parallel plates (Navier-Stokes in rectangular coordinates). [19]

$$\lim g\left(\frac{r_p}{r_b}\right) = n \tag{15}$$

$$\left(\frac{r_p}{r_b}\right) = m \tag{16}$$

n	m	model
1	0	circular pipe
1.5	1	parallel flat plate
1.0 to 1.5	$0 < m < 1$	annulus

Table 3: Relationship between radii [19]

Where r_p is the radius of the plunger and r_b the radius of the barrel. If the radii are rather similar in size "n" 15 becomes $n = 1.5$ and the $r_p/r_b \approx 1$ which therefore describes the flow between two parallel flat plates.

Figure 16 displays the velocity profile between two non moving plates. The velocity profile is symmetrical, parabolic shaped and has its maximum at the half distance between plunger and barrel. The velocity is zero at both walls since no wall is moving and no-slip is assumed.

Integrating Equation 14 twice, leads to:

$$u = \frac{1}{2\mu}\left(\frac{\partial p}{\partial x}\right)y^2 + C_1 y + C_2 \tag{17}$$

Since the change in pressure is constant over the length of the plunger $\partial p/\partial x$ becomes $-\Delta p/l$ and $u = 0$ for $y = 0$ (at the surface of the plunger) and $y = h$ (at the surface of the barrel) for non-moving plates. Including these boundary conditions in Equation 17:
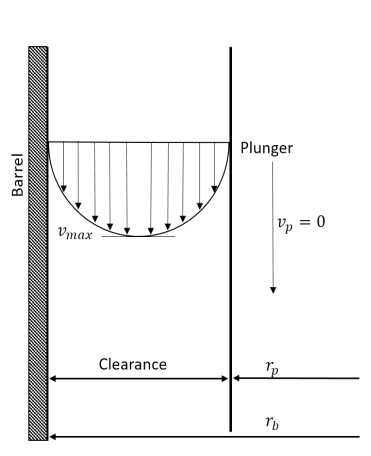
Figure 16: Fluid velocity profile, no moving plunger

BC's		
I	$y = 0$	$u = 0$
II	$y = h$	$u = 0$

Table 4: Boundary conditions for flow between two plates

$$u = -\frac{1}{2\mu}\frac{\Delta p}{l}y(y - h) \tag{18}$$

To determine the volumetric flow rate, it is necessary to integrate Equation 18 with respect to A the Area, while assuming that the annulus is wrapped into a rectangular with height of h and length of $2\pi r$:

$$Q = \int_A u\partial A = \int_0^{2\pi r}\int_0^h -\frac{1}{2\mu}\frac{\Delta p}{l}y(y - h)dydz = \frac{\pi r h^3 \Delta p}{6\mu l} \tag{19}$$

Which is a variation of the basic slippage Equation [6]:

$$B = K\frac{PD^x C^z}{\mu L} \tag{20}$$

Comparing Equation 19 and 20 it can be seen that $z = 3$ and $x = 1$. Further Describing K as a constant, which includes $\pi/3$, P or Δp is the pressure across the plunger, D or r as the diameter or radius of the pump, C or h as the clearance μ as the fluid viscosity and L as the stroke length.

3.2.3. Flow between static barrel and moving plunger (Navier-Stokes)

Figure 17 displays the fluid velocity profile for an upward moving plunger while the fluid is forced back from the top to the bottom. It furthermore illustrates the change in velocity profile. The maximum is shifted to the left, towards the barrel and the velocity at plunger has the opposite direction compared to the max velocity of the fluid flow. The velocity of the fluid at the plunger is the same as the plunger velocity due to the no-slip condition.
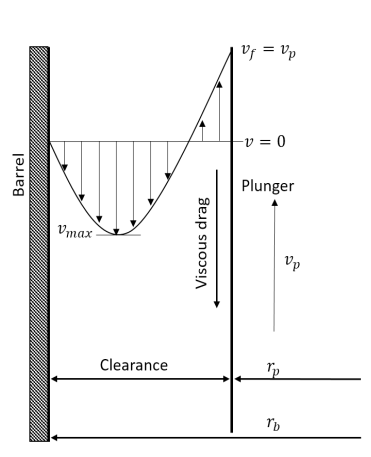
Figure 17: Fluid velocity profile, upward moving plunger

Figure 15 and Figure 17 clearly indicate a change of the parabolic velocity profile as a result of the moving plunger. The moving plunger and its velocity effect the amount of slippage volume and therefore need to be taken into account.
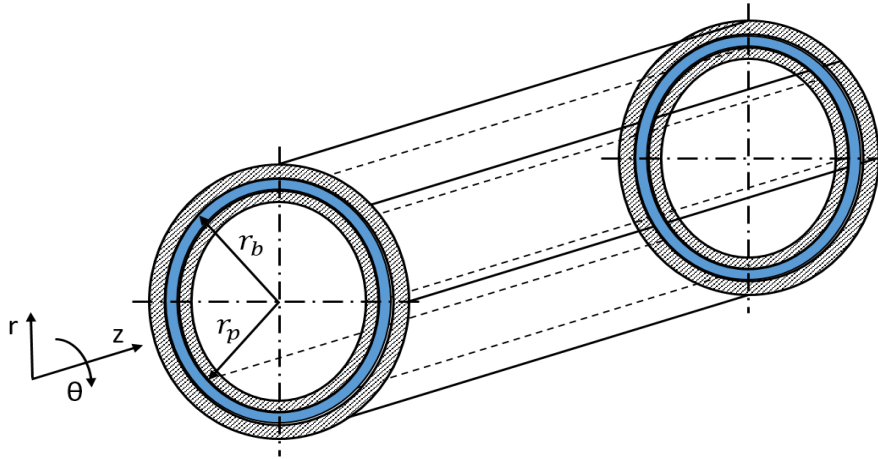
Figure 18: Flowrate in pipe annulus

Figure 18 displays in blue the annulus or clearance between plunger and barrel. The z coordinate directs in flow direction, for r: $0 < r < r_b$ where r_p is the plunger radius and r_b is the barrel radius.

Starting with the same assumptions, which lead to Equation 17, but now using cylindrical coordinates.

$$\frac{dp}{dz} = \frac{\mu}{r}\frac{d}{dr}\left(r\frac{dv_z}{dr}\right) \tag{21}$$

23

Where z is the direction of the flow and r is the radius. Integrating twice with respect to r leads to:

$$\frac{dp}{dz}\frac{r^2}{4\mu} + C_1 \ln r + C_2 = v_z \tag{22}$$

BC's		
I	$r = r_b$	$v_f = 0$
II	$r = r_p$	$v_f = -v_p$

Table 5: Boundary conditions for flow in annulus

The integration constants can be found by using appropriate boundary conditions. The first is that the fluid velocity at the barrel is zero and the second is that the fluid velocity at the plunger is the same as the plunger itself. Since the plunger is moving upward the velocity points in the negative z-direction. Both boundary conditions are summarized in Table 5 and lead to following Equation 23.

Annular velocity profile during upstroke:

$$v_z = \underbrace{\frac{dp}{dz}\frac{1}{4\mu}\left((r^2 - r_b^2) - \frac{r_b^2 - r_p^2}{\ln r_b - \ln r_p}(\ln r - \ln r_b)\right)}_{static-part} + \underbrace{v_p \frac{\ln r - \ln r_b}{\ln r_b - \ln r_p}}_{dynamic-part} \tag{23}$$

Where z is in the direction of the fluid flow, μ the viscosity of the fluid, r the radius from r_p to r_b, r_b is the radius of the barrel, r_p is the radius of the plunger, v_p is the velocity of the moving plunger and v_z the velocity of the fluid. The equation is derived for an upward moving plunger, it can be seen that an upward moving plunger adds additional losses to the static-part. If the plunger would move downward the dynamic part would change its sign and reduce the amount of total slippage.

Equation 23 clearly indicates the dependency of the fluid velocity profile to the moving plunger. It furthermore displays the difference between the *static* part which is a function of geometry and pressure and the *dynamic* part which is a function of the plunger velocity and the geometry.

3.2.4. Flow between two non-moving plates (Dimension Analysis)

Besides analytical or numerical solutions of the problem using the Navier-Stokes equation, it is also possible to derive the problem via Dimension Analysis. Therefore it is necessary to list all influencing variables, which have an effect on the problem. The $Buckingham - Pi - Theorem$ than states how these variables are combined with each other.

The instruction to the $Buckingham - Pi - Theorem$ and the following derivation is based on [14].

According to [14] it is essential that the later on proposed equation, which could be a function involving many variables is balanced:

$$u_1 = f(u_2, u_3, ..., u_k) \tag{24}$$

This means that u_1 has to have the same dimensions as any term which stands alone on the right side of the equal sign. This equation could than be rearranged to dimensionless products (pi terms) which were first introduced by Buckingham. [14]

$$\prod_1 = \phi(\prod_2, \prod_3, ..., \prod_{k-r}) \tag{25}$$

The first step and probably the hardest is to define all influencing factors which require deep knowledge of the problem. Variables, which do not have a direct impact on the solution could falsify the dimension analysis. Same fluid mechanical assumptions were made as mentioned before. The pressure difference of a fluid flow between two parallel plates depends on [14]:

$$\Delta p = f(C, \mu, L, v) \tag{26}$$

Saying that the pressure difference is a function of the distance between both plates, C (in our case the clearance between plunger and barrel), the viscosity of the fluid μ, the length of the plates L and the velocity of the fluid flow v.

The second step is to express these variables in their basic dimensions in terms of length L, time T and mass M:

$$\Delta P \hat{=} ML^{-1}T^{-2}$$

$$v \hat{=} LT^{-1}$$

$$L \hat{=} L$$

$$C \hat{=} L$$

$$\mu \hat{=} ML^{-1}T^{-1}$$

The third step of the $Buckingham - Pi - Theorem$ is the evaluation of the required number of Pi-terms. The number of variables is $k = 5$ and the number of reference/basic dimensions is $r = 3$ resulting in two necessary PI-terms $k - r = 2$

Step four and five is the selection of repeating variables and their multiplication with one of the non repeating variable. According to step three, this needs to be done twice, resulting in two Pi-terms.

$$\prod_1 = \Delta p v^a \mu^b C^c \tag{27}$$

Δp... non-repeating-variable
$v^a \mu^b C^c$... repeating-variables

We now express each variable of 27 with is basic dimensions as expressed in the second step above.

$$M^0 L^0 T^0 = ML^{-1}T^{-2}(LT^{-1})^a(ML^{-1}T^{-1})^b(L)^c \tag{28}$$

Comparing the exponents on the left side of the equation with the exponents of the right side of the equation leads to an equation system.

$$\text{for M: } 0 = 1 + b$$

$$\text{for L: } 0 = -1 + a - b + c$$

$$\text{for T: } 0 = -2 - a - b$$

Solving this equation system results in: $a = -1$, $b = -1$ and $c = 1$ which furthermore leads to:

$$\prod_1 = \frac{\Delta p C}{v \mu} \tag{29}$$

This step needs to be done again for the second Pi-term while Δp (the non repeating variable) is exchanged with L.

$$\prod_2 = L v^a \mu^b C^c \tag{30}$$

Which results in:

$$\prod_2 = \frac{L}{C} \tag{31}$$

When combining the Pi-Terms according to Equation 25, this results in:

$$\frac{\Delta p C}{v \mu} = \phi\left(\frac{L}{C}\right) \tag{32}$$

The Buckingham PI-theorem does not state the form of the function ϕ, but knowing that the delta pressure across the length is proportional to the length L this results in:

$$\frac{\Delta p C}{v \mu} = K\left(\frac{L}{C}\right) \tag{33}$$

Where K is a constant. Rearrangement of Equation 33 to v and multiplying with the area, where the flow has to pass through ($A = D_p \pi C$) leads to the flow rate.

$$Q = Av = K \frac{\Delta p C^3 D_p \pi}{\mu L} \tag{34}$$

Comparing now the basic slippage Equation 20, the equation derived by the analytical solution of the Navier-Stokes problem 19 and the solution of the dimension analysis 34. It can be seen, that all three equations state that the volume flow rate increases with increasing pressure Δp, increasing clearance C (by the power of three) and plunger diameter D_p. It decreases with an increase in viscosity μ and plunger length L.

Furthermore, it can be seen, that all three approaches assume laminar steady state fluid flow between two parallel plates. The viscosity is held constant and assumed to follow Newtons law, the fluid is incompressible and the surface of the plates is smooth.

However, the petroleum industry deals with fluids which do not behave like Newtonian fluids and are also sometimes compressible due to the dissolved gas in it. Abrasive materials are roughening the surface which results in a loose of the validity of smooth surfaces.

Still, these assumptions are valid enough to predict fluid loss in small clearances.

3.3. Historic and Current slippage models

Most of the nowadays used slippage models follow the basic slippage Equation 20 and just differ in their constants and exponents. The following equations are based on both theory and experiments. However, it is difficult to set up a general formula if the experimental setup is limited to specific testing conditions. Therefore and due to the variation of testing- and operating conditions finding an accurate and in general applicable slippage model is often difficult.

Historic Slippage models

Developer	Formula
Robinson (1935)	$B_R = 1.596 * 10^7 \dfrac{PDC^3}{L\mu}$
Davis and Stearns (1944)	$B_{DS} = 4.17 * 10^6 \dfrac{PC^{1.9}(d_2^2 - d_1^2)}{d_2^{0.1} L\mu}$
Robinson and Reekstin (Published 1960)	$B_{RR} = 5.61 * 10^6 \dfrac{PD^{0.7}C^{3.3}}{L\mu}$
ARCO-Harbison Fischer (2000)	$B_{AH} = 870 \dfrac{PDC^{1.52}}{L\mu}$

Table 6: Historical slippage equations without consideration of pumping speed [6]

Robinson, 1935

The first slippage model was developed by Robinson in 1935. His test setup was a 4000 feet deep pump without standing valve and an averaged clearance which was about 0.0055 inch. Data from the tests were not published. Necessary information e.g. the plunger size, fluid viscosity or the test setup was not recorded either. Chambliss [6] tried to reconstruct Robinsons test setup and derived following equation which is stated in Tabel 6.

Davis and Stearns, 1944

Stearns performed the first investigation on the influencing factors of slippage. According to him geometry of the plunger (length, diameter and fit), the surface of the plunger, the differential pressure across the plunger, the viscosity of the oil and the density of the oil influence the slippage rate of a Sucker Rod Pump. Stearns performed tests with a plain 2.25 inch plunger. He performed several tests and published the slippage rate for each condition in a table [20]. With the help of Davis theoretical approach Stearn published an equation to describe slippage losses [6].

Table 6 states historical slippage equations. All models above are based on the basic slippage Equation 20 with varying constants and exponents. However non of these models take the pumping speed as an influencing variable into account.

Developer	Formula
Cox, Nickens and Lea [21]	$41.96uDC + \dfrac{83745DC^3P}{L\mu}$
Theta Oilfield Services [22]	$[(0.14SPM) + 1]453\dfrac{DC^{1.52}P}{L\mu}$

Table 7: Historical slippage equations with consideration of pumping speed [2]

Table 7 states slippage models which also take the pumping speed into account. Where u is the plunger velocity in ft/sec and spm the strokes per minute. Furthermore, it can be seen that the constants and exponents of the models mentioned in table 7 also vary. The table furthermore illustrates that the *plunger velocity term* is just added to the basic slippage equation, but this confirms to the Navier-Stoke solution of flow in the annulus, which can be seen in Chapter 3.2.3.

As has been reported by Chambliss [6], most of the former used slippage models refer to the basic slippage model. The inaccuracy of the old models motivated him to perform additional tests. He performed tests at one pump to be able to change the coefficients of the old models and therefore update the old inaccurate models.

Chambliss (2005):

$$B_{New} = 654\frac{DPC^{1.52}}{L\mu} \tag{35}$$

In order to define a new equation he performed tests with one specific pump at different speeds varying from $5.08 - 9.76 SPM$ with increments between $1.2 - 1.9 SPM$. No change of plunger type or pressure difference/setting depth was mentioned. Freshwater was used as liquid. Experimental setup:

Pump intake pressure	50 psi
Pump discharge pressure	1760 psi
Plunger length	48 in
Plunger Diameter	2.001 in
Pump Clearance	0.009 in
Viscosity	0.764 cp (at 90° F)

Table 8: Pump parameters of test well [6]

It should be noted, that no change in pressure difference across the pump was made due to the fixed setting depth. Furthermore, one plunger and one type of fluid viscosity was used for the experiments. Additionally, it was mentioned, that Equation 35 lacks of tests at different pump speeds and pump types.

4. Data statistics and model algorithm

4.1. Slippage-model establishment

Equation 23 and Table 7 clearly indicate that the old and historical slippage model 20 requires an update. Both illustrate that the volume of slippage is also a function of the plunger velocity.

During the data processing for this thesis, a model was established, which includes the old slippage model 20 and an additional term for the plunger velocity.

During the analysis of the measured data, it was found out that the model to describe slippage needs additional constants to fit the data. These constants were used to minimize the error between model and measured data and to maximize the fitting process.

4.1.1. Slippage model

The Matlab-code is presented in the Appendix A

$$f = @(k)(k(1) * v * C * D * t) + k(2) * t * P * \frac{C^{k(3)} * D^{4-k(3)}}{\mu^{k(4)} * L} \tag{36}$$

The @ symbol describes Matlabs' function handle to call the function which follows the @. The constants k(1), k(2), k(3) and k(4) represent the values which should be varied to maximize the fit of the function to the given data. The other constants are f the volume loss per stroke [m3̂] (later called q), v as the velocity of the plunger in [m/s], C the clearance in [m], D the plunger diameter in [m], t the time required for one stroke, P is the pressure difference across the plunger μ is the apparent viscosity of the fluid in [Pas] and L is the plunger length in [m]. Equation 36 displays both the old slippage model on the right hand side and the dependency of the plunger velocity on the left hand side. Constant 1 and 2 are multiplied, whereas constant 3 and 4 contribute as exponent for their specific variables. Furthermore, it can be seen that also the viscosity has an exponent although the dimension analysis does not state one. During the data analysis it was found out, that the tests performed with water and those performed with Xanthan Gum did not correlate at all. An exponent for the viscosity was introduced. (Detailed explanation later.)

The dimension analysis in Chapter 3.2.4 displays that the sum of the exponents of clearance C and diameter of the plunger D has to be four. Consequently, the exponent of D is equal to 4 minus the exponent of C.

4.1.2. Optimization of the new slippage model

The main reference of this chapter is the documentation of Matlab [23]. Navier Stokes and the dimension analysis, provide the basis to establish an equation, which describes downhole pump losses. Prior to the optimization-algorithm, three constants were used to optimize the function. For better error minimization, a fourth exponent (exponent for viscosity) was introduced.

The equation is based on the assumption that the fluid behaves Newtonian, therefore and also to minimize the error, an additional constant was introduced as an exponent of the viscosity to describe downhole pump losses in a more accurate way.

Talking about optimization, the aim of this thesis is the establishment of an equation, which describes losses as best as possible. Therefore, it was necessary to select an optimization-algorithm that suits the problem best. The function, which was required to

be optimize is called "objective function". An objective function is a function, which needs to be either maximized or minimized in order to suit the problem. There are many solvers available to minimize objective functions.

Objective Type Solvers (Scalar)[24]:

- fmincon

- fminunc

- fminbnd

- fminsearch

- fseminf

- fzero

Scalar objective functions accept scalars, vectors or matrices as input arguments and provide scalars as outputs. For the objective function, in this case, both vector and scalars were used as input arguments and scalars were required as output arguments (coefficients). Most of the solvers are based on different algorithms. Depending on the problem, it is necessary to choose an appropriate algorithm. Sometimes and if the computation of the outcome is not that calculating time intensive it is possible to compare the results of different solvers and different algorithms. Next to the definition of initial points, also called starting points, of the algorithm it is required to specify what should be optimized. In this case $k0$ defines the initial point vector. The length of this vector is also an input argument for the optimization-algorithm, because it is used to determine the number of variables which the function accepts.

$$k0 = [124; 0.0026; 3; 0] \tag{37}$$

4.1.3. Fminsearch vs. Fmincon

Two algorithms were used to optimize the result of the objective function. *Fminsearch* was used first. The algorithm sufficiently minimized the error in measuring each point. The coefficients calculated by the algorithm and the model were then combined and used to calculate slippage.

In most of the cases the error was small, but in some of the cases, the equation, based on *fminsearch*, predicted losses higher than the maximum produceable volume which the pump would be capable to produce. In other words, predicted losses were higher than Q_{max} (1) this would result in a downflow of liquid. Since artificial lift systems should add energy and help to lift the fluid and because this outcome does not make sense the solver *fmincon* was chosen. The target was to achieve a prediction, which has a maximum value $= Q_{max}$. This means in the worst case our pump does not produce any liquid and the well is not flowing anymore. Therefore we defined the max loss as Q_{max}

$$target = min(loss(:, 1), maxVol) \tag{38}$$

Q_{max} is in this case described by *maxVol*.

By the definition of this equation, it is defined that the loss is not higher than *maxVol*. So in the case that our measured loss would be higher than *maxVol* the min function would assign the *maxVol* as the target value. But this is unlikely. SSECF is the *Sum Squared Error Cost Function*. It describes the sum of the squared error. The error is the difference

between our measured or assigned data (target) and the outcome for a specific point of the objective function f(k).

$$SSECF = @(k)sum((target - f(k)).^2) \tag{39}$$

We now need to define further input arguments for the *fmincon* solver:

$$lb = [-20000, -20000, 1, -20000] \tag{40}$$
$$ub = [20000, 200000, 4, 20000] \tag{41}$$

Lb and *ub* describe the lower and upper bound of the constants. The solver tries now to calculate constants within the range of the boundaries.

According to the dimension analysis above we know that the product of $C^{k(3)} * D^{4-k(3)}$ should have a maximum exponent of 4. Therefore we can assign boundaries to keep the exponent below a certain value.

A and *b* describe linear inequality constraints, *Aeq* und *beq* describe linear equality constraints but those were not used.

$$A = [] \tag{42}$$
$$b = [] \tag{43}$$
$$Aeq = [] \tag{44}$$
$$beq = [] \tag{45}$$

Nonlcon describes nonlinear constraints which are specified by an objective function. The nonlinear constraint is used to keep the outcome of the result below the maxVol which is required as mentioned before.

$$nonlcon = @(k)deal(f(k) - maxVol, []) \tag{46}$$

4.1.4. Fmincon

The main reference of this chapter is: [25]

With all these input arguments *fmincon* calculates the constants required to establish the slippage model.

$$[abc] = fmincon(SSECF, k0, A, b, Aeq, beq, lb, ub, nonlcon) \tag{47}$$

With [abc] as the output vector.

$$a = abc(1) = k(1) \tag{48}$$
$$b = abc(2) = k(2) \tag{49}$$
$$c = abc(3) = k(3) \tag{50}$$
$$e = abc(4) = k(4) \tag{51}$$
$$\tag{52}$$

The solver *fmincon* is based on constrained nonlinear optimization-algorithms. Aim of this optimization-algorithms is to find local minima for the function f(x) with the input vector x. In our case, we want to minimize an objective function with an input argument vector and want to have 4 scalars as an output result.

$$\min_{s}\{q(s), s \in N\} \tag{53}$$

The *fmincon* algorithm is based on the trust region approach. The basic idea of this approach is that you start at a specific point x in n-space which has a specific value for f(x) and you want to proceed in a direction where the result is smaller.

Since many functions f are quite complex, this approach uses a simplified function called q to mirror the behavior off *f*. With s as step rate we try now to minimize the outcome of q in the trust region more precisely in the neighborhood N around x.

The value of f(x) should be smaller as the value f(x+s). This describes a negative gradient and the direction to a minimum. If this would be not the case the neighborhood would be narrowed and the direction of s would be changed. According to [25] the key approach is now to choose an appropriate reflective function q and how to define and change the neighborhood N. q is stated as the first two terms of the Taylor approximation for F at x for the trust region problem

$$min\left\{\frac{1}{2}s^T Hs + s^T g \text{ such that } \|Ds\| \leq \Delta\right\} \tag{54}$$

Where H is the matrix of the 2$^\text{nd}$ derivatives (also called Hessian matrix), D is a diagonal scaling matrix and g describes the 1$^\text{st}$ derivative of f at a point x. Matlabs optimization toolbox tries to keep the trust-region sub-problem two dimensional and computes the subspace S.

Maintaining two-dimensionality allows even for large scale problems easy and fast solving of Equation 54. Describing the two-dimensional subspace as linear space spanned between s_1 and s_2, where s_1 follows the direction of the gradient g and s_2 is described by the direction of the negative 2$^\text{nd}$ derivative of $s_2^T Hs_2 < 0$ or as an approximation of the solution of $Hs_2 = -g$.

According to [23] the unconstrained minimization using trust regions could be described and summarized by four steps:

1. Define and formulate the two dimensional trust region sub-problem

2. Solve Equation 54 by calculating all Eigenvalues of the Hessian matrix and the application of a Newton process

3. If the function outcome of the trial-step $f(x + s) < f(x)$ is smaller than the origin then $x = x + 2$ and Δ (scalar) is adjusted

This steps repeat so long until convergence, a pre-defined result or the maximum number of iterations is reached. The result of this process is illustrated in table 20 for different starting points and input parameters.

4.2. Data fitting and analysis

The main references of this chapter are [26] and [27].

This chapter describes the required steps to process data from the measurement until the final use in an equation. Table 16 describes a process of averaging a repetitive measurement. A repetitive measurement is a multiple measurement of the same quantity. Averaging is a necessary statistical process. Furthermore it is necessary to describe the data variance, the measurement error and the error between measured and calculated data.

Statistical analysis

It is important to say that measurements never display the truth, there are always errors even if the error is small. This further means that the engineer must be aware of how the measurement should work, how data is collected and what are the necessary steps to process the data.

The measurement never displays the truth, according to [27] this could be expressed as:

$$\text{measured value} = \text{true value} \pm \text{error} \tag{55}$$

This describes that the error is the difference between the true value and the measurement. It is not possible to eliminate the error completely but with a clear understanding of the measurement devices it is possible to minimize systematic errors. If the error is randomly distribute it is necessary to perform multiple measurements and average the result which minimizes the error. [27]

Statistical tools to analyze the measured values are the sample variance, the sample standard deviation and the standard error of the mean.

$$s^2 = \frac{\sum_{i=1}^{n}(x_i - \overline{x})^2}{n-1} \tag{56}$$

Where s^2 describes the sample variance which is an estimate of the variance σ^2. The sample standard deviation could be expressed as the square root of the sample variance.

The measurements of the produced mass per stroke are based on an averaging process of approximately five strokes per testing condition. The researcher recognized an variation of produced mass under the same condition, this required an averaging of the measurements. To validate the mean it is then necessary to calculate the variance. Which could be described as:

$$s_{\overline{x}} = \frac{s}{\sqrt{n}} \tag{57}$$

When the number of observations is large the error of the estimated mean becomes small. [27]

To describe the degree of correlation between measured and calculated data it is necessary to calculate either the covariance or the correlation coefficient. The correlation coefficient describes a scaleless covariance [26]. According to [26] the correlation coefficient between two sample sets y_1 and y_2 (in our case the sample sets represent measured and modeled data)is then defined as:

$$r = \frac{\sum(y_1 - \overline{y_1})(y_2 - \overline{y_2})/(n-1)}{s_1 s_2} \tag{58}$$

5. Experimental design and test setup

5.1. Pump Test Facility

The Pump Test Facility (PTF) at the Montanuniversitaet Leoben, was designed to investigate equipment under near-field conditions. Since equipment tests in the field are cost intensive and would disturb the normal production the PTF is designed to simplify those tests. The PTF furthermore provides the ability of low risk and low costs tests of new equipment and is therefore an essential link between laboratory measurements and field applications. A schematic sketch of the test facility is in Appendix B.

5.1.1. Pump-Jack

Due to spatial limitations in the laboratory, the installation of a normal pump jack was not possible, therefore adaptions were made to simulate real-life conditions. A linear servo drive was used to simulate the movement of the pump jack. The servo drive with electronic position-, velocity- and torque control system moved a skid upward and downward.

   Supplier: *Bosch Rexroth AG* [28]
Motor-Type Specification: *MAD130C-0150-SA-M2-AH1-35-N1*

   Connected to this asynchronous motor with variable speed drive is a two-meter long spindle which drives a skid/sledge. Attached to skid there is the polished rod. As a fact that the pump is installed in a 10m deep shaft, the pump plunger is directly connected to the polished rod. The combination of the linear servo drive, variable speed drive, spindle, skid and polished rod makes it possible to simulate the behavior of a normal pump jack. The variable speed drive allows, within the system boundaries, pump velocities between 0 and $10spm$, with linear or sinusoidal velocity profiles.

   The PTF uses a 6 5/8" casing as a pressure vessel, which has a maximum length of 10 m. Under real-life conditions sucker rod pumps are sometimes installed with little inclination due to the borehole orientation. Therefore it is also possible to incline the PTF up to 30°, to test under inclined conditions. Previous to the measurements every joint was sealed with special equipment. The pump was then pressurized up to 35 bar to observe leaking joints. No leaks were detected.
   The pressure vessel is pressured via a centrifugal pump.

   Supplier: *SAER ELETTROPOMPE* [29]
Pump-Type Specification: *HT2-V18-B14-100L*

   This centrifugal pump creates the necessary intake pressure for the pump and therefore simulates the reservoir pressure. The pump is capable of 9 *bar* intake pressure and delivers up to $4 - 13$ m³/h.
   These conditions allow simulating operating conditions up to 500 m pump setting depth. Additionally, the fluid temperature can be adjusted up to $60°C$. Operating temperature of the pump and fluid were ambient temperatures, during the measurements a minor but not significant temperature increase was recognized.

5.1.2. Specification of the used pump

This chapter describes the pump, which was used to investigate the volumetric efficiency evaluation at PTF Leoben.

The pump used for the measurements has the following designation **30-225 RHBC**. ”**30**” describes the tubing size, the inside diameter of the barrel, of $3^{1/2}$ in, ”**225**” describes the basic pump bore diameter of $2^{1/4}$ in, ”**R**” stands for a rod pump, ”**H**” describes the type of barrel and in this case a heavy wall barrel for metal plunger pumps, ”**B**” describes the location of the seating assembly and in this case it is bottom seated via ”**C**” a cup seat assembly.

The pump is bottom seated to have equal pressure distribution at the outside of the barrel compared to top anchored pumps. This avoids ballooning of the barrel and therefore a change in geometry. A change in geometry would cause a clearance variation, which effects the amount of slippage volume in an unpredictable way. These plastic seat cups are used to fix the stationary part of the pump to avoid unwanted barrel movement. Another function of these cups is to prevent fluid to flow back from the tubing to the wellbore. [3]

In conclusion at the measurements a **Stationary barrel bottom anchored rod pump** was operated.

Plungers

To be also able to predict losses as a function of clearance, plungers with different diameter were chosen:

1	Harbison Fischer - Spray metal pin end plunger with diameter of **57.15 mm**. Specification: *59-252L4-6*. Plunger length: **1630 mm**; Status: new
2	Harbison Fischer - Spray metal pin end plunger with diameter of **56.497 mm**. Plunger length: **1630 mm**; Status: severely grooved surface
3	Harbison Fischer - Spray metal pin end plunger with diameter of **56.855 mm**. Plunger length: **1630 mm**; Status: minor grooves on surface
4	FARR Plunger with diameter of **57.099 mm** Plunger length: **1645 mm**
5	Soft packed plunger, with *Martin Wiper Composition Rings*[30] with a diameter of **55.502 mm** with the dry and not swelled sealing elements; Plunger length: **1205 mm**

Table 9: Plungers used for the measurements

Table 9 displays the used plungers for the measurements. Pictures of the used plungers can be found in the Appendix B. Plunger 1 to 3 are *Harbison Fischer* [31] spray metal pin end plungers. The first plunger was not used before, is without grooves or other damages and is therefore new. The second plunger has a clear decrease in diameter compared to the 1st one.

(a) Plunger 2

(b) Plunger 3

(c) Plunger 5

Figure 19: Pictures of plunger 2, 3 & 5 (Table 9)

The 2nd and 3rd plunger were provided by the *OMV Austria Expl.&Production GmbH* and were used before. They furthermore show severe surface grooves and corrosion since they were used before. According to *OMV Austria Expl.&Production GmbH* the 2nd plunger was used for around 976 days and produced a cumulative volume of 42555 m^3 at a pump speed of 4.85 *spm*.

The 3rd plunger was also used before and shows minor scratches, almost no corrosion and a slight decrease in diameter compared to the new 1st plunger. According to *OMV Austria Expl.&Production GmbH* the 3rd shall be presumed to be used for about 56 days and produced about 1074 m^3 at a pump speed of 2.3 *spm*.

The 4th plunger is a FARR plunger also provided by *OMV Austria Expl.&Production GmbH* and manufactured by *Muth Pump* [32]. The FARR-plunger is used especially in sandy and solid rich environments. The plunger prohibits, due to its cone shape outlet at the top, that sand enters the gap between the plunger and the barrel. Which significantly reduces the risk of sticking and drastically reduces the wear of the pump. As a result, the lifetime of the pump is increased by 300 to 600 % according to [32].

The 5th plunger is a soft-packed plunger also provided by *OMV Austria Expl.&Production GmbH*. The plunger was used earlier but was equipped with new sealing elements before the measurements for the thesis. The plunger is equipped with swell-able sealing elements. These sealing elements swell when in contact with fluid and allow for maximum tightness between barrel and plunger. This sealing elements perform best at high temperatures and for higher gravity oils. Usually, these plungers are used when sand is produced to be able to protect the interface between plunger and barrel. These plungers in addition increase the volumetric efficiency, due to the enhanced tightness in the barrel.[30]

5.2. Test program

The target of this thesis is the evaluation of the volumetric efficiency of sucker rod pumps. Chapter 3.3 describes old and new slippage models. Models, which are the result of field tests for specific conditions. If the test program is too limited and lacks in variation of influencing factors, it is hard to describe the volumetric efficiency with a generalized equation. Under previous tests performed at the PTF [2] it has been found that these models severely underestimate losses. In general, the theory and current models predict the trend of downhole pump losses but the underestimate the magnitude. Measurements show that theory only predicts a tenth of the losses compared to what was measured.

This is why it was necessary to perform additional measurements to predict downhole losses. To be able to create a model for a wide application it was essential to vary the operating conditions as much as possible. For each test it was assumed that the pump was filled completely, the presence of gas is excluded, eccentricity is assumed to be zero since the tests were performed under vertical conditions and the temperature influence is also assumed to be zero.

The basic slippage equation describes slippage as a function of pressure, plunger- diameter and length, viscosity and clearance:

$$B = K \frac{P D^x C^z}{\mu L} \tag{59}$$

During the measurements all these dependencies were varied. Following test program was used to evaluate the losses:

Pumping speed		Pressure difference across plunger				
$[spm]$	$[mm/min]$	$[bar]$
		$21 - 6$	$27 - 5$	$29 - 4$	$33 - 3$	$37 - 2$
0.5	1650	$\overline{M_{11}}$	$\overline{M_{12}}$	$\overline{M_{13}}$	...	
1	3300	$\overline{M_{21}}$	$\overline{M_{22}}$	...		
1.5	4950	$\overline{M_{31}}$	...			
2	6600	...				
2.5	8250					
3	9900					
3.5	11550					
4	13200					
4.5	14850					
5	16500					
6	19800					
7	23100					
8	26400					
9	29700					
10	33000					

Table 10: Test program

Table 10 states the variation of pumping speed and pressure change. The table indicates that pumping speed was varied between 1 and 10 spm with increments of 0.5 for the first half and 1 spm for the second half. For each velocity the pump was operated at five different pressure differences. For each velocity and pressure difference five to seven strokes were performed. The actually produced mass was then averaged for each speed and pressure difference.

The actually produced fluid was pumped into a 100 L tank attached to a load cell on the top. This arrangement made it possible to measure the total mass produced by a single stroke.

$$\overline{M} = \frac{1}{n} \sum_{i=1}^{n} M_i \tag{60}$$

Pressure variation:

$\Delta p =$	p_o-	p_i
$15 =$	$21-$	6
$22 =$	$27-$	5
$25 =$	$29-$	4
$30 =$	$33-$	3
$35 =$	$37-$	2

Table 11: Pre-defined pressure differences

Table 11 displays the predefined pressure differences across the plunger. Five different intake and discharge pressure were chosen to test the pump. p_i describes the intake pressure of the pump, which is created by the centrifugal pump mentioned in Chapter 5.1.1. p_o is the outlet pressure of the pump which is controlled by a two-point regulator. The two point regulator opens and closes the pressure relief valve if a specified value is exceeded or undershot, which results in a smooth opening and closing operation.

This predefined pressure was set in the software, the actual intake and outtake pressure were separately measured and recorded.

$$\Delta p = \frac{\int_a^b \Delta p_{(t)} dt}{b - a} \tag{61}$$

$\Delta p_{(t)}$ describes the pressure difference over the time of one stroke. The pressure was averaged for each stroke, where a and b describe the beginning and the end of the stroke.

Table 10 describes the test program for each plunger.

5.2.1. Modified fluids

To predict losses as a function of viscosity it was essential to perform tests with different viscosities. The basic slippage Equation 20 states that slippage is inverse proportional to the viscosity, which means the higher the viscosity the less the amount of volume is lost. The basic slippage equation furthermore shows a linear relationship between viscosity and slippage.

To be able to investigate the influence of viscosity, three different viscosities were used for each plunger mentioned above.

Each plunger was tested with freshwater and two additional more viscous fluids. Some viscous fluids were used for two plungers. Following the experiments, each viscous fluid was processed with the *Chandler Engineering Viscometer* [15] to find out the viscosity.

As viscousifying agent *S-ES BIO XG* [33] was added to water, which is a natural polymer.

6. Data evaluation

6.1. Rheological-model of Xanthan Gum

According to [34] the rheologic behavior of xanthan gum is clearly non-Newtonian. The research clearly indicates that xanthan gum solutions are highly pseudo plastic. It further shows that the viscosity is rather low for high shear rates and gel-like for low shear rates.

Rheometer

According to [15] the used viscometer has following specifications:

Sample Container Volume	350 mL
Shear rate accuracy	+/- 0.01 RPM
Torque Accuracy	+/- 0.5 dial reading from 1 to 260 degrees

Table 12: Specifications of Chandler Engineering viscometer Model 3500 [15](modified)

Constant	Value
k_1	386
k_2	0.01323
k_3	1.7023

Table 13: Constants of Chandler Engineering viscometer Model 3500 [15]

Example dial reading for viscosity used for plunger two Table 9:

Theta (dial reading)	1	1.25	1.5	1.75	2.25	2.5	3	3.5	4.5	5.5	7	10
RPM (n)	1	2	3	6	10	20	30	60	100	200	300	600

Table 14: Dial reading (example)

Measurement uncertainties were observed during the viscosity measurement of the fluids. Especially for low viscous fluids at low rpm the dial reading was unstable.

Table 14 displays the dial readings for given RPM. With respect to table 12 which indicates a torque accuracy of +/- 0.5 it is clear that for low rpm the dial reading is difficult. Which in addition to the unstable reading may lead to severe measurement errors. This is why the lower readings were excluded for the viscosity models. Dial readings above 30 RPM appeared to stable and good.

During the measurements of this thesis, eight different Xanthan gum solutions were used. All solutions were measured with a rotational viscometer Chandler viscometer Model 3500 [15] (see Appendix B). Density measurements did not indicate a change in density after the addition of Xanthan gum.

Rheological-model of used Xanthan Gum mixtures

During the viscosity measurement uncertainties were detected. For low rpm and low viscosity solutions the dial reading was not stable. This non-stability influences the viscosity model. Instabilities for dial reading up to 30 rpm were observed. For higher rpm (>30 rpm) and higher viscous solutions the dial reading was stable.
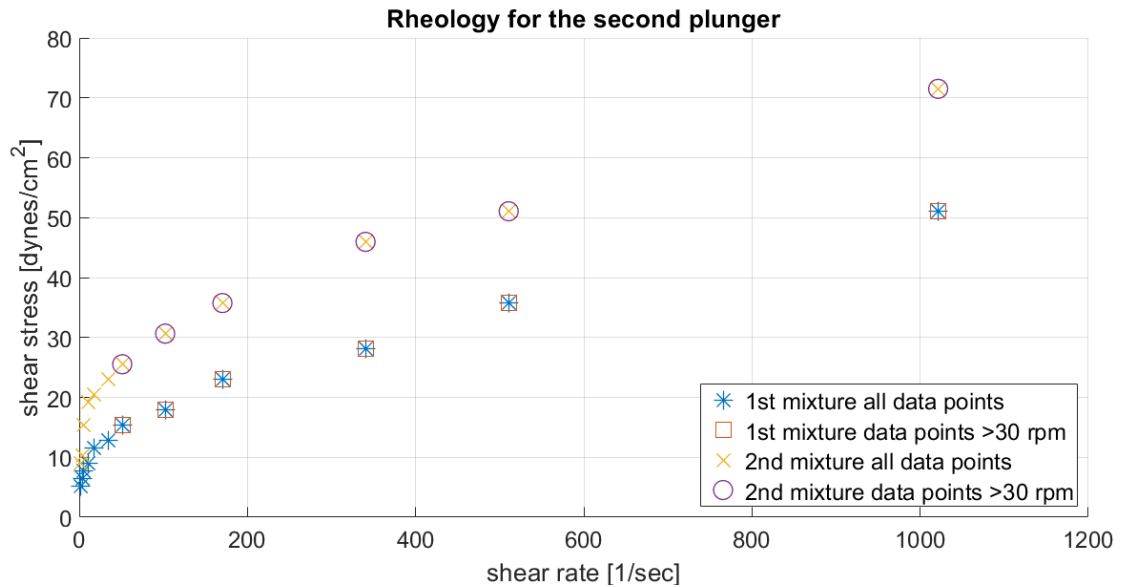
Figure 20: Rheology for the second plunger

Figure 20 displays two different viscosity solutions which were used for the 2nd plunger which was mentioned in Table 9. The graphic clearly indicates non-Newtonian behavior which could be interpreted as shear thinning fluid. Figure 20 furthermore displays all measurements points for both fluids and measurements points above 30 rpm. As mentioned before the dial reading was unstable for rpm < 30, nevertheless and also with the exclusion of the lower shear rates, the viscosities still show shear thinning properties. Measurement uncertainties for lower rpm made it impossible to describe a yield value of the y-axis. This is why the viscosity is assumed to behave like a pseudoplastic Power-law fluid.
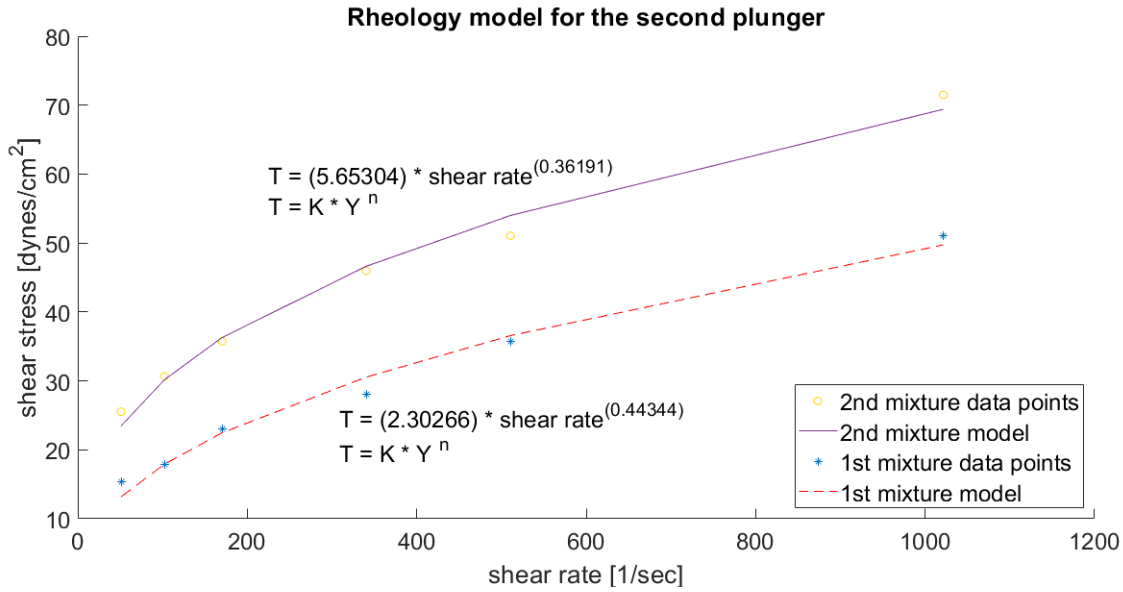
Figure 21: Rheology-model for the second plunger

Figure 21 displays the Power-law model for the two mixtures used for the 2nd plunger. The graphic displays a flow behavior index n (*degree of non-Newtonian-ity*) of 0.443 for the higher viscous fluid and 0.361 for the lower viscous fluid. Both are less than one($n < 1$) and therefore indicate shear thinning properties. The consistency indices of K are 2.30 and 5.65 for the higher and lower viscous fluid. The used fluid with higher Xanthan Gum concentration has a higher consistency index but a lower flow behavior index. The amount of Xanthan Gum in solution has therefore an effect on both constants.
According to [18] the more Xanthan Gum is in solution the higher is the hydrostatic pressure and the yield point of the fluid, which results in a higher consistency index. On the other hand a higher concentration means a higher pseudoplastic behavior and therefore a reduction of the flow behavior index.
In a log-log plot of shear rate versus shear stress the exponent n would describe the slope of the model. Since the fluid is shear thinning and it is not possible to assign a single viscosity for every condition the viscosities needed to be matched to correct condition.
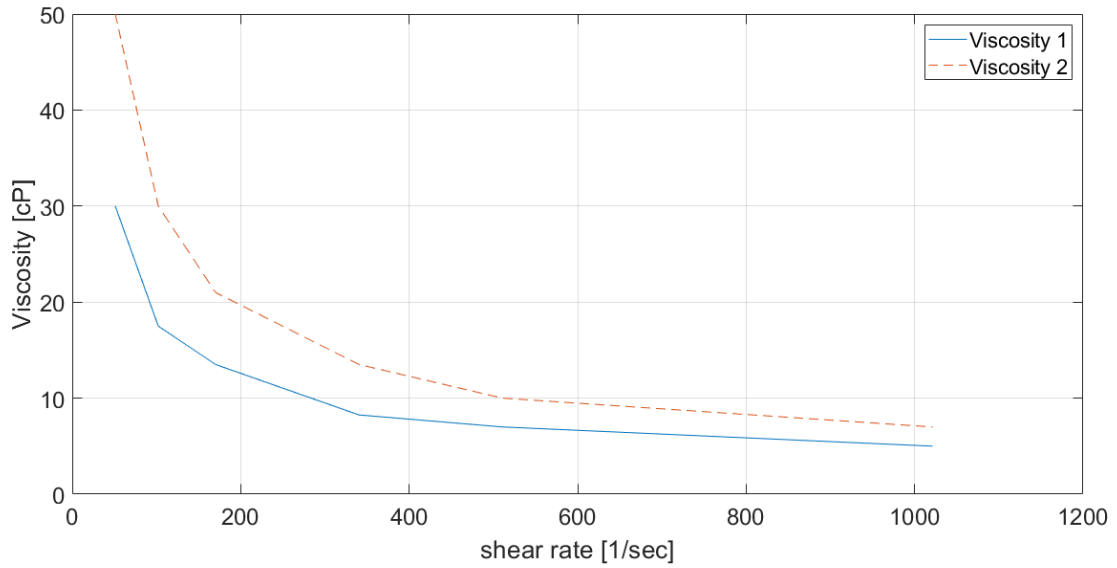
Figure 22: Viscosity for the second plunger

Figure 22 clearly displays a relationship between shear rate and effective viscosity. The shear rate is defined as $\dot{\gamma} = \frac{du}{dy}$. Since the plunger of the pump is moving with different velocities and the clearance is not the same for each plunger it was necessary to match the right viscosity to its shear rate. Consequently it could be stated that: $\dot{\gamma} = \frac{du}{dy} = \frac{\text{Plunger velocity}}{\text{Clearance}}$. Shear rates for every velocity and clearance were calculated. The correct viscosity was selected and matched and therefore every plunger velocity and clearance has its own viscosity.

6.2. Data evaluation and test results

Chapter 5.2 describes the experimental setup to gather the necessary data. The following chapter explains the data collection, processing steps, the evaluation and interpretation of the collected data.
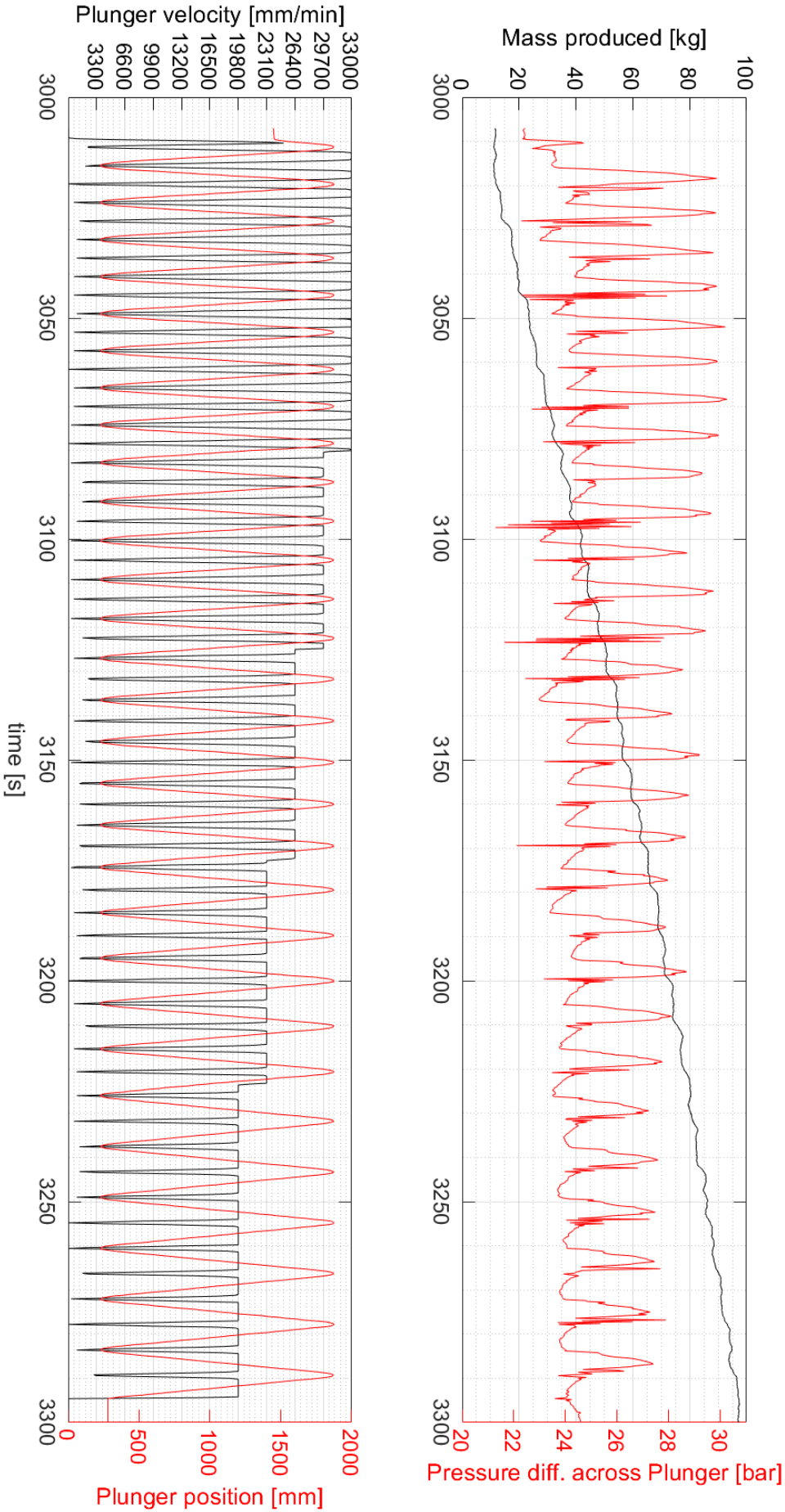
Figure 23: Data recording of plunger two (Table 9)

Data recording

Figure 23 displays the way of recording data. The upper graph shows the produced mass of liquid on the left side in [kg]. The right side of the upper graph displays the pressure difference across the plunger [bar].

The graph below illustrates the plunger velocity in [mm/min] and the plunger position in [mm].

The pressure curve is illustrated by the red curve of the upper graph. With an increase in plunger position, during the upstroke, the pressure increases. This pressure increases until a certain predefined threshold is reached. Figure 23 illustrates one specific pressure difference defined in Table 11. If this threshold is reached the two-point pressure regulator opens and releases fluid. Which is illustrated by the black curve on the upper graph. It shows that after a certain threshold is reached the produced mass of fluid increases. The produced mass curve is step wise shaped which is a result of the production after each stroke of the pump.

The black curve in the lower graph illustrates the plunger velocity. It shows plunger velocities between ten and six spm with 1 spm increments (Table 15). It furthermore illustrates that the plunger has a constant velocity during the up- and down stroke of the pump. The velocity of the plunger is zero at the top and bottom of each stroke, resulting in a not constant velocity profile as shown in Figure 24.

SPM	1	2	3	4	5	6	7	8	9	10
mm/min	3300	6600	9900	13200	16500	19800	23100	24600	29700	33000

Table 15: Plunger velocity
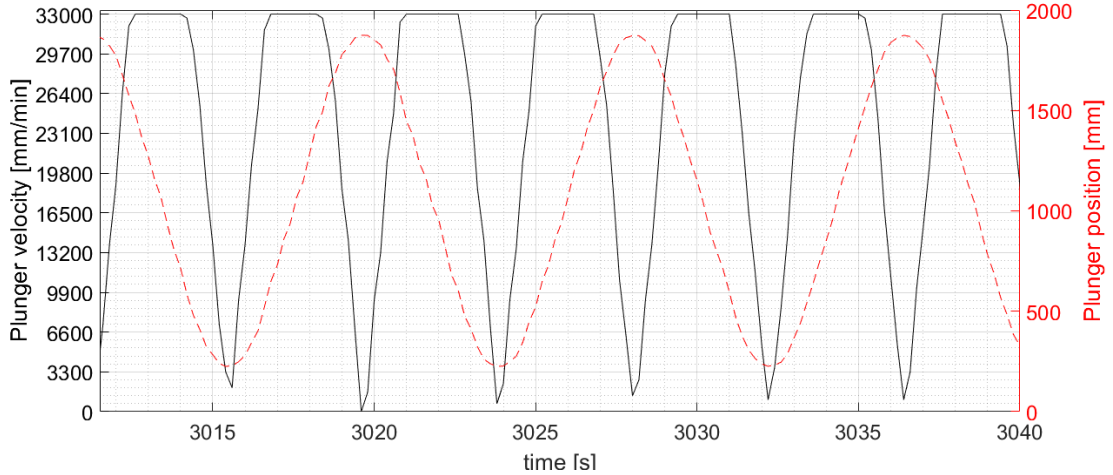
Figure 24: Velocity profile of the plunger

Figure 24 shows an acceleration of 30 mm/s^2 at the start of each stroke until the predefined velocity is reached. Not visualized in the graph is the dead time at the top and bottom of each stroke of about 0.05 s. The red curve in the lower graph of Figure 23 and in Figure 24 illustrate the plunger position and stroke length (dashed line). Stroke length was chosen to be between 225 mm as lower boundary and 1875 mm as upper boundary, which results in a total stroke length of 1650 mm. The stroke length is then used to calculate the maximum produceable volume ($Q_{max} = 4.2L \stackrel{\wedge}{=} 4.2kg$) as shown in Equation 1, which

was then compared with the actually produced volume to calculate the losses per stroke.

$$Q_{\text{loss per stroke}} = Q_{max} - Q_{actual} \tag{62}$$
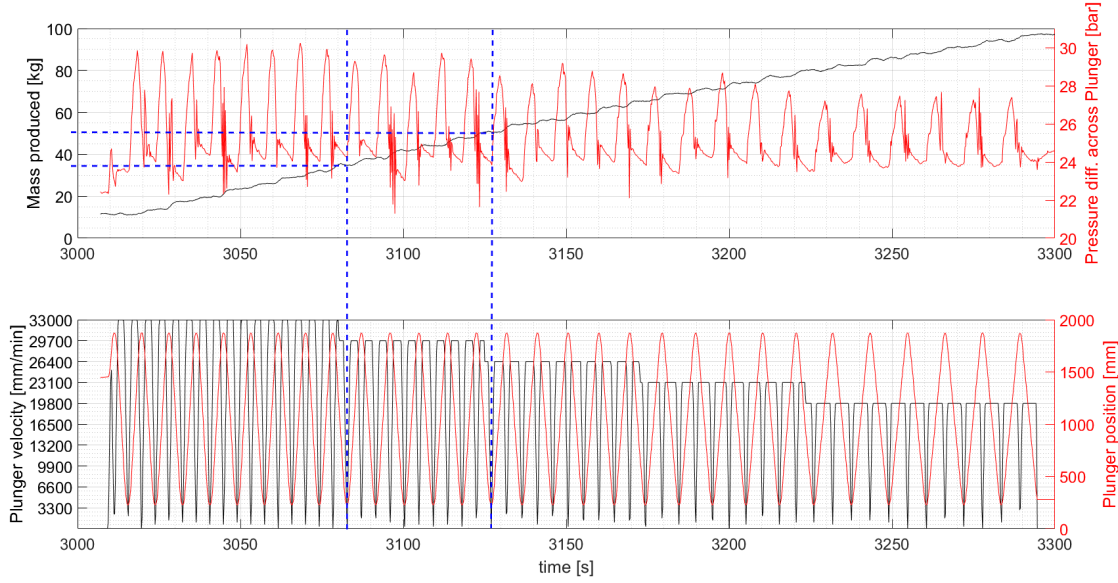
Figure 25: Evaluate produced mass

To be able to calculate the losses per stroke, Figure 25 was used to pick the beginning and end of a stroke sequence for one velocity.(marked by the blue dashed lines). *Matlab - Mathworks [35]* was used to pick the points. The range where the points were picked was then automatically processed.

This range delivered the number of strokes, the average pressure difference over each stroke and the mass of liquid at the start and end of the range. This was then converted to an average produced mass per stroke.
An example is shown below for plunger two 9:

[mm/min]	Δp	Mass p.s.[kg]
33000	16.876	3.5379
29700	16.494	3.3266
26400	16.116	3.6801
23100	15.925	3.3824
19800	15.674	3.0096

Table 16: Picked mass for plunger two (Table 9)

Table 16 states a part of the record. The table represents the stroke velocity in $[mm/min]$, the pressure difference in $[bar]$ across the plunger and the already average mass per stroke in $[kg]$. For single strokes the produced mass varied between $\pm$ 0.5 kg. This was known beforehand and was taken into consideration. Therefore at least 5 strokes were performed for each condtion to reduce the magnitude of the error. If the error is randomly distribute it is necessary to perform multiple measurements and average the result which minimizes the error. [27]

Measured data - Harbison Fischer plunger two Table 9

The following figures represent Table 16:
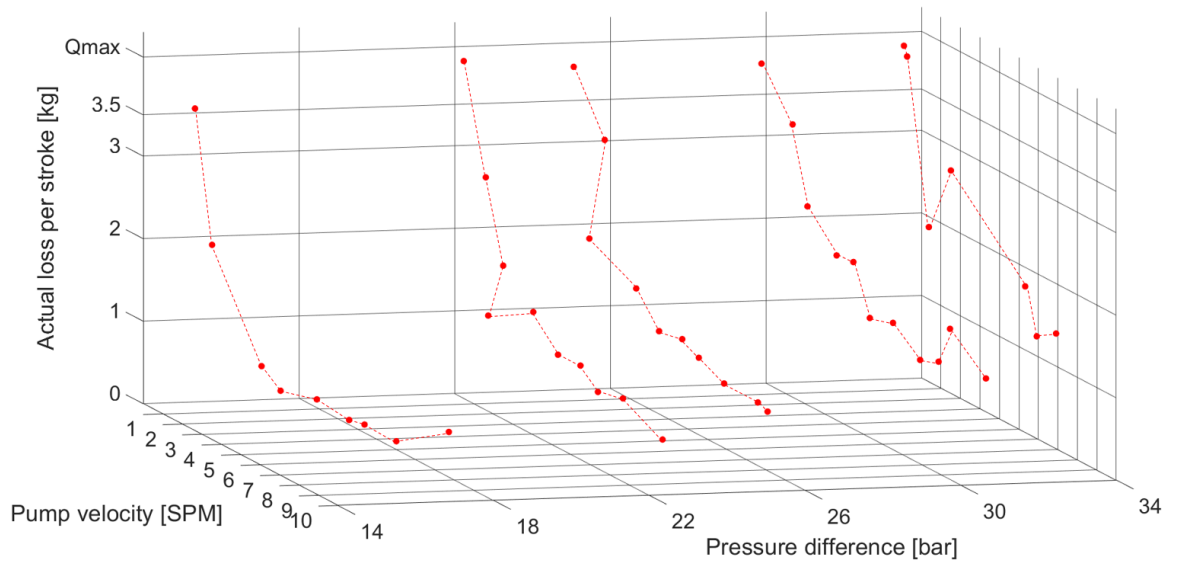
Figure 26: Measured losses - Plunger two (Table 9)

Figure 26 illustrates the losses of plunger two, Table 9, with a plunger to barrel clearance of $2.23749e - 04$ m and an average diameter of $56.497\ mm$.

Figure 26 displays the pump losses also called slippage under several operating conditions. The figure clearly indicates lower losses for a lower pressure difference and higher losses for a higher pressure difference. This means with an increasing pressure difference the losses also increase. This behavior is also described by all old slippage models. $q_{loss} \propto \Delta P$.

It could be further seen that the losses per stroke increase with a decrease in strokes per minute. For the lower pressure differences a sharp increase in loss is recognized with a decrease in pump speed. In total, the cumulative losses increase the faster the pump is moving. This velocity dependency made it necessary to include a velocity term in the slippage equation.

In addition the figure illustrates losses almost up to 100% in the back of the plot. Low pumping speeds and high pressure differences contribute both to an increase of slippage.

Measured data - cont'd - Harbison Fischer plunger two Table 9
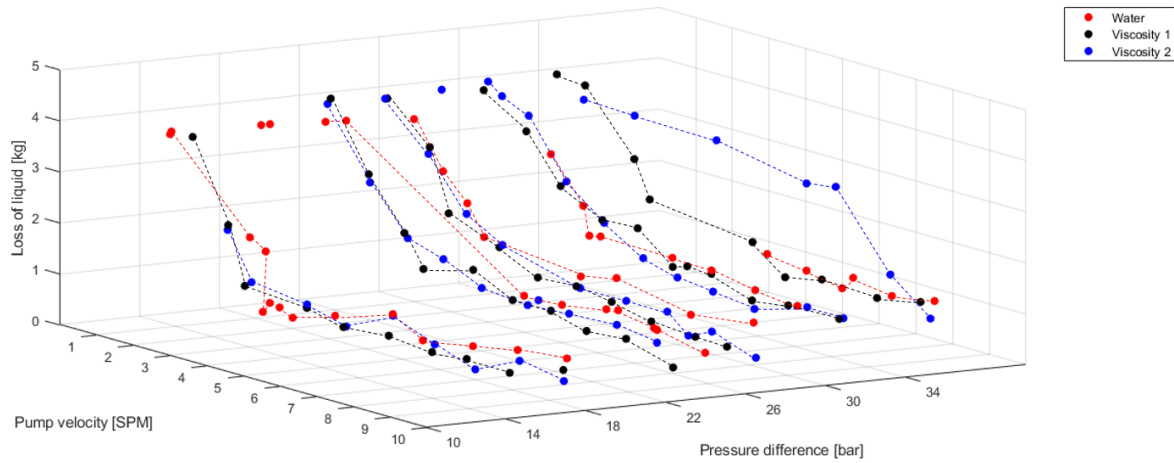
Figure 27: Measured losses - Plunger two (Table 9) with two modified fluids.

Figure 27 displays the losses per stroke of Plunger two Table 9 for water and for two modified fluids. The viscosities for the two modified fluids are illustrated in Figure 22. 2D side view plots of Figure 27 can be found in Appendix B.

Basically the following applies: the higher the viscosity of the fluid, the lower the losses per stroke are. It can be seen that the losses, at lower speeds and lower pressures, are smaller for higher viscous fluids compared to the losses of less viscous fluids. Furthermore, the same behavior as in Figure 26 can be recognized. The losses drastically increase with lower pumping speeds and also increase with higher pressure differences.

At the right side of the curve, the blue dots in the back illustrate really high losses for almost every pumping speed. This could be a result of the combination of large clearance, higher viscosity compared to water and the first modified fluid and to the large pressure difference across the plunger, although the old slippage equation would predict the opposite. But it can not be ruled out that these points are measurement errors. The way of measurement was not changed, but such high losses indicate a different and not expected behavior.

Further, it could be stated, that almost every modified fluid measurement point indicate lower losses compared to water.

Modeled data vs. measured data
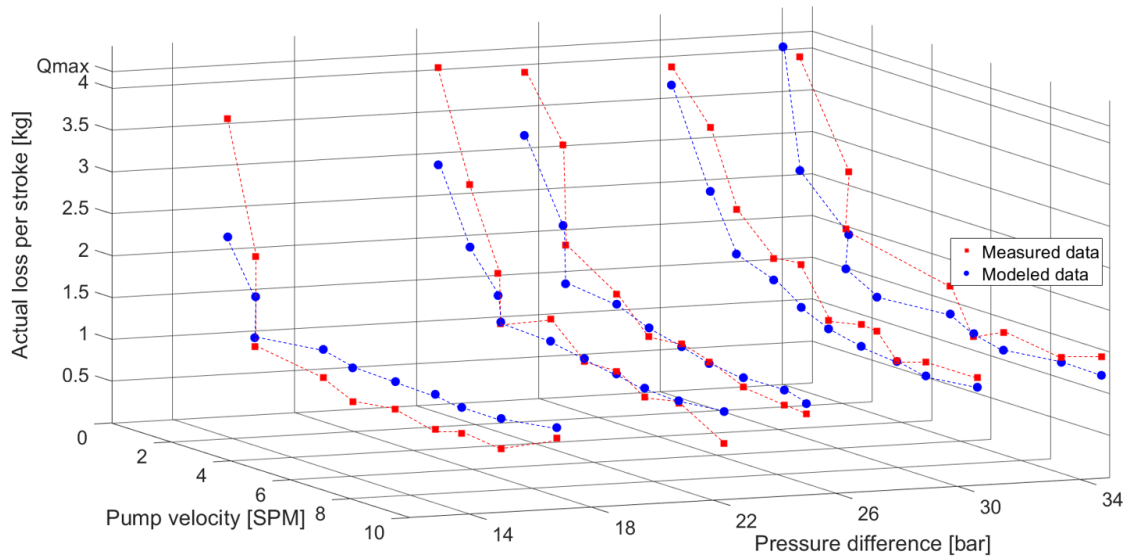
Figure 28: Modeled data vs. measured data

Figure 28 displays the modeled and measured data for the second plunger and modified fluid 1. The figure visualizes that, the model is not so accurate for lower pressure differences but increases in preciseness at higher pressure differences. For the pressure difference around 15 *bar* and 1 *spm* it clearly underestimates the loss. For the data points at around 22 and 26 *bar* pressure difference, the error is rather small except for the lowest pump velocity.

Furthermore, the model shows a constant and smooth decline in loss from 1 to 10 *spm* for every pressure difference.

The trend of the model is clearly depicted. The losses per stroke decrease with an increase in velocity and increase with an increase in pressure difference. 2D side view plots of Figure 28 can be found in Appendix B

Measured data - Soft-Packed Plunger
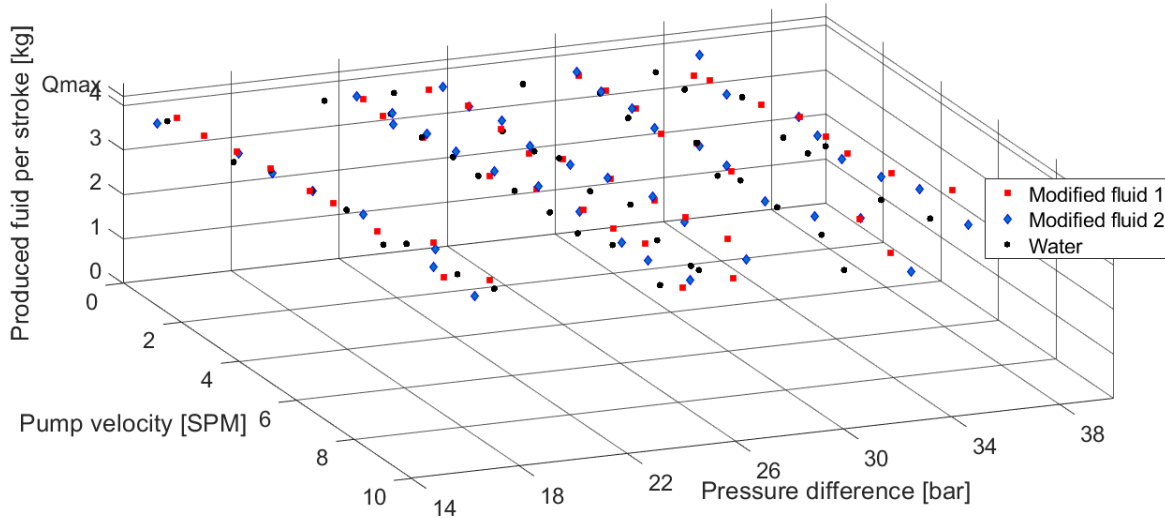
Figure 29: Measured losses - Plunger five (Table 9) with two modified fluids.
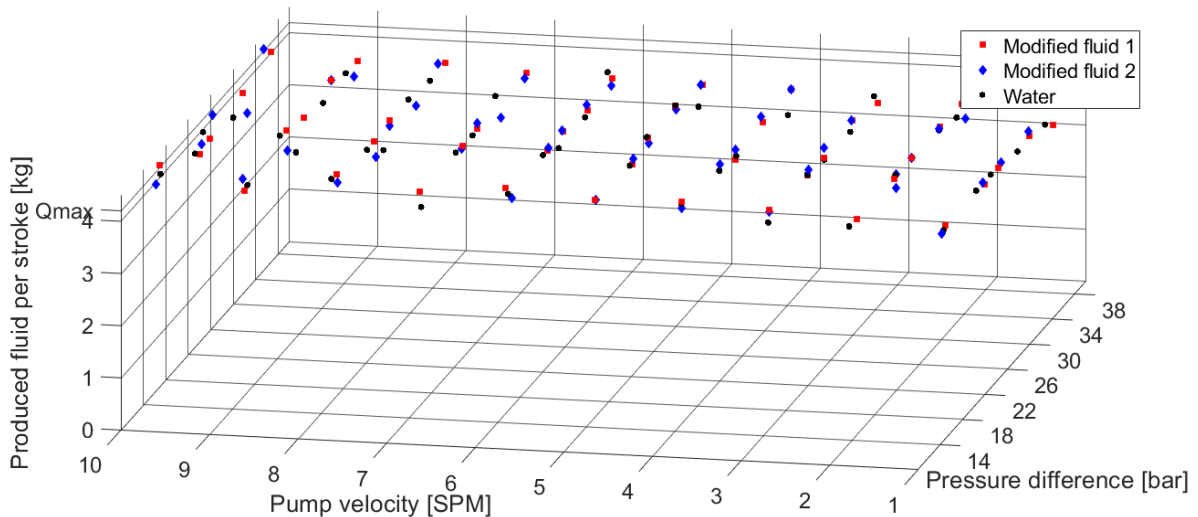
Figure 30: Measured losses - Plunger five (Table 9) with two modified fluids.

Figure 29 and Figure 30 display the losses of the soft-packed plunger (Plunger five Table 9). Two figures were used for better illustration. Both show almost no dependency on pump velocity and pressure difference. Once the sealing elements of the soft packed plunger are swollen, they ensure tight sealing. Almost no losses are recognized. A detailed look on the dependency of pressure difference, shows higher losses with an increase in pressure difference.

Compared to Figure 27 and Figure 26 the soft-packed plunger shows almost linear behavior and seems unaffected by an increase or decrease in speed and pressure. This is why the soft packed plunger was not included for the development of the new slippage model.

Model comparison

During research on the Montanuniversitaet Leoben it was found out that the current slip-
page models do not predict the actual losses of the measurements performed at the PTF-
Leoben. Before starting with the tests following steps were taken:

1. Pressure testing the facility to ensure tightness of all joints. The pump itself is bottom
   anchored in the tubing. Previous to the measurements the pump was pressurized up
   to 40bar and no significant pressure drop was observed.

2. Furthermore, every additional equipment-part was tested and checked to ensure
   proper function.

3. The same barrel and tubing was used for all measurements to ensure equality.

After excluding all potential errors concerning the Pump Test Facility, measurements
were performed as described before. During the measurements itself no malfunctions or
any other inconsistencies of the pump were observed. The data recording was without
errors.

Still big discrepancies between the old models and the measured slippage volume was
detected.
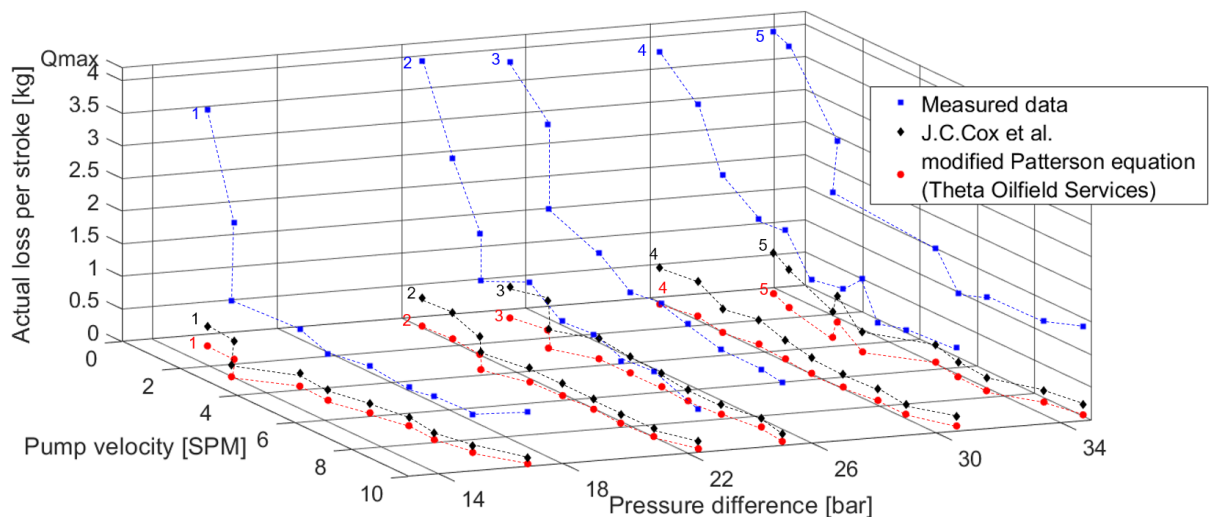
Figure 31: Old models vs. measured data

Figure 31 displays the the discrepancies between two models and the measured data.
The two models by J.C.Cox et al. [21] and Theta Oilfield Services [22] are displayed.
The graphic illustrates differences up to 700% for low velocities. The accuracy increases
with increasing velocity but only due to the lower losses of the measurements itself. Both
models underestimate the impact of pumping velocity severely, displayed with almost no
change. J.C.Cox et al. predicts the losses for high pressure differences and low velocities
better compared to the Theta Oilfield Services. 2D side view plots of Figure 31 and 31 can
be found in Appendix B.

Test conditions

Plunger clearance [m]	$2.375 * 10^{-4}$
Plunger diameter [m]	$0.0567 * 10^{-2}$
Plunger length [m]	1.63
Stroke length [m]	1.65
Pressure [bar]	$14 - 35$
Fluid viscosity [Pas]	0.005
Plunger velocity [SPM]	$1 - 10$
Pump fillage [%]	100

Table 17: Testing conditions

Table 17 displays the testing condition for the comparison of the three models Figure 32 and also for Figure 31. For the two old models the test parameter-units and values were converted.
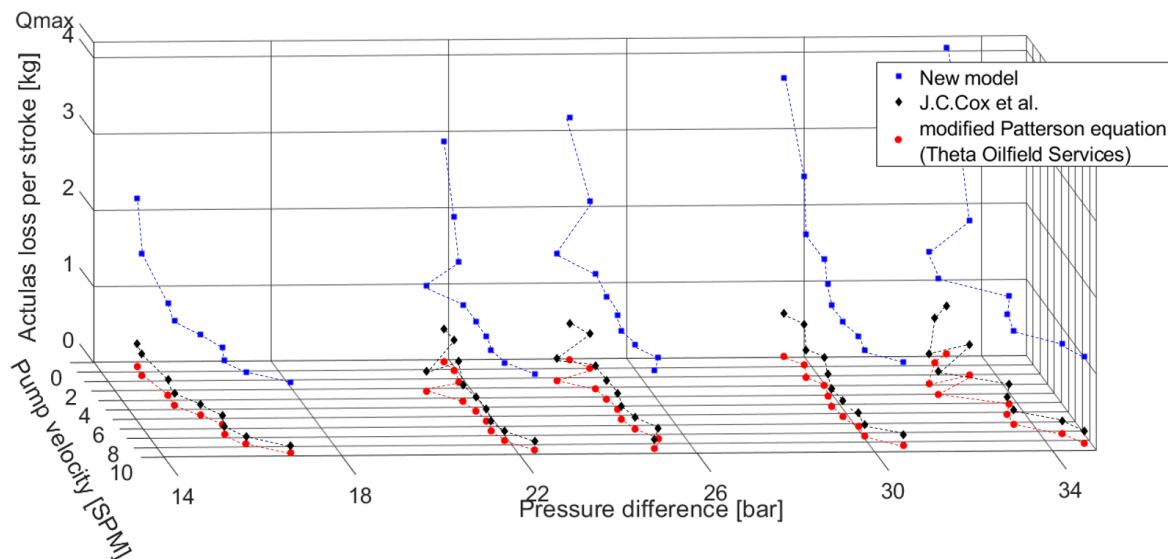
Figure 32: New models vs. measured data

Figure 32 displays the differences between the new model and the old models. The new model which is developed on the base of the measurements and the two other models.

6.2.1. Statistical analysis of modeled data

Plunger one to four 9 do have a normal metal to metal interface. All four plungers are similar in their construction. Plunger one to three are the same, they only differ in diameter, which is a result of the previous usage. Plunger four (FARR plunger) differs a little in his structure at the top compared to the other three. The cone shape outlet of the plunger is used to prohibit sand settling between plunger and barrel but it also influences the fluid dynamics at the top. The FARR plunger also shows different results, which is shown later. Compared to the other four the soft-packed plunger completely differs in his setup. The swell able rings, almost completely tighten the interface between plunger and barrel. The soft packed plunger does not show a similar behavior in volumetric efficiency and was therefore excluded and not considered for the model.

To evaluate the accuracy of the model it was necessary to interpret and describe the error of the model. The error, as stated before, is the difference between true and measured value or in this case the difference between measured and calculated value (based on the model). The error furthermore does not only describe the model error it also displays measurement errors. [27]

The modeled error is displayed in the error histogram.
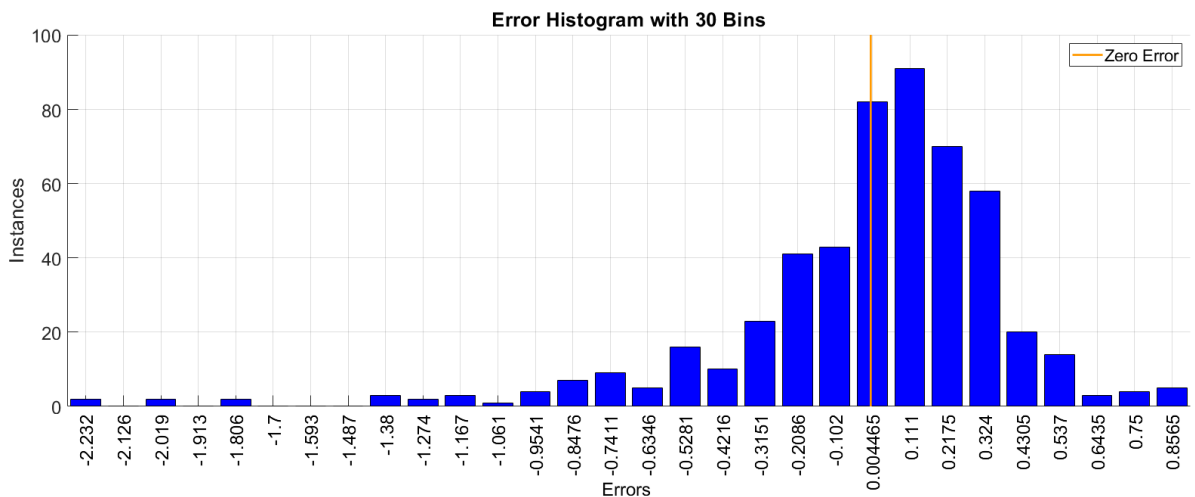
Figure 33: Error distribution for all four plungers

Figure 33 displays the error distribution for a model which includes four plungers as input parameters. (soft-packed plunger excluded) The figure plots the number of instances on the y-axis and the error on the x-axis. The histogram furthermore represents an error which is Gaussian or normal distributed. The error is distributed with 30 bins around zero.
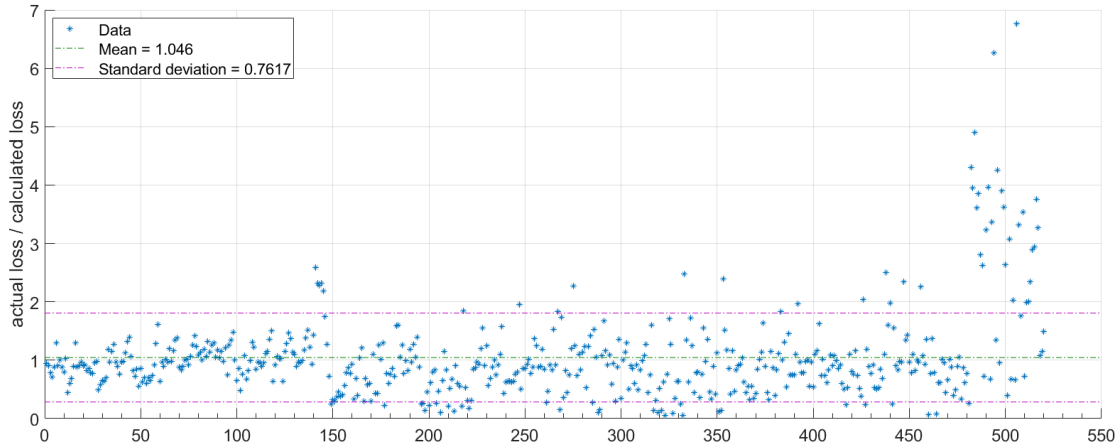
Figure 34: Model error for all four plungers

Figure 34 displays the error of *actual loss divided by the calculated loss* on the y-axis and the number of elements on the x-axis. Where *loss = max.Volume - actually produced Volume.* The number of elements describe measurement points for the plungers. The y-axis furthermore represents the error of the model, meaning a y-axis reading of two says the model fails to predict the truth by 200%. Ideally, all data points should lay around 1, since if the error is low the fraction between actual and calculated loss should become 1. The figure legend displays an overall mean of 1.046. This means that the overall error is 4.6% over the entire chosen data set. The standard deviation, the deviation from mean is 0.761.

Plunger (Table 9)	Range
Plunger two	1 - 147
Plunger one	148 - 316
Plunger three	317 - 481
plunger four	482 - 520

Table 18: Number of elements of (Figure 34)

Table 18 describes the range of data points which belongs to each different plunger. In general, around 150 data points were chosen to describe each plunger. This is a result of the previous mentioned test program. Unfortunately, most of the FARR plunger measurements for the higher viscosities failed. As a result of this, these points were not considered for the model.

Furthermore Figure 34 describes outliers at around 140 (x-axis). These outliers describe an un-normal low modeled loss and un-normal high actual loss. This high actual loss is basically a result of a higher pressure difference compared to the data points before and furthermore a result of the slow pumping speed. In this case the model is not able to predict such high losses and fails to model the true value. At the end of the plot, at around 480 (x-axis) data points form the FARR-plunger are displayed. The model also fails to predict the losses of the FARR-plunger.
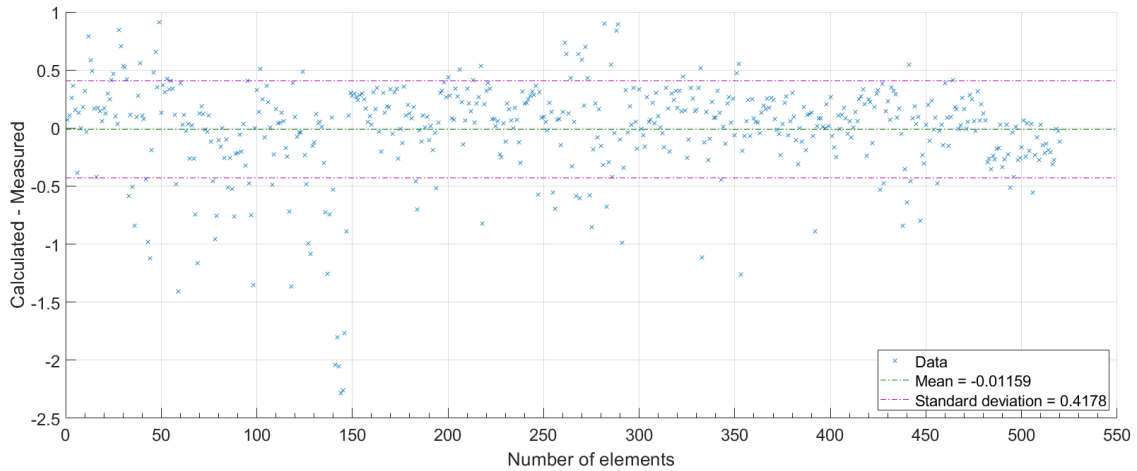
Figure 35: Model error for all four plungers

Figure 35 displays difference between Calculated and measured data. The result in each point should be zero if the error is very small. Since there is always an error the result of the difference lays around zero. An average of this error was calculated which is about -0.011, which describes a total error of around 1%nt over the entire data point set and a standard deviation of about 0.4178. Figure 35 furthermore displays the same outliers at around 140 and 480 (x-axis reading). These errors describe the high-pressure losses of plunger two and the inaccuracy of the model to predict the FARR-plunger losses.

Data-Set	Input
1	All 4 plungers
2	W/O FARR plunger
3	New plunger
4	Plunger 5695
5	Plunger 5681

Table 19: Data-Set input argument

Data-Set	CorrC	$\overline{x}$ of div.	Std. of div.	$\overline{x}$ of subtr.	Std. of subtr.	Constants			
						a	b	c	e
1	0.9086	1.0456	0.7617	-0.0116	0.4716	1.7776e+04	16.3506	1.8110	0.3073
2	0.9104	0.9139	0.4362	-9.564e-04	0.4297	1.7622e+04	17.1343	1.8203	0.3089
3	0.8733	1.0110	0.5849	-6.310e-07	0.2648	1.0318e+04	81.8957	1.8308	0.1046
4	0.8834	1.0011	0.5028	-6.117e-06	0.3035	8.1793e+03	92.8747	1.9189	0.1714
5	0.8572	0.9963	0.3378	-0.071	0.6146	2.0861e+04	73.9455	2.0811	0.2951

Table 20: Coefficient comparison

Table 19 is linked to table 20 and displays the first column of table 20. Table 20 displays now different results for different input arguments. The table displays from left to right the correlation coefficient ($CorrC$) the mean ($\overline{x}$ of div.)and standard deviation *Std. of div.* of Figure 34, the mean ($\overline{x}$ of subtr.) and standard deviation *Std. of subtr.* of Figure 35 and the coefficients for the model. The table shows different input arguments. In the first line all four plungers (except the soft-packed plunger) were used to feed the model. The second line displays input arguments for the model excluding FARR plunger and soft packed plunger. From the third to the last line the plungers were evaluated separately.

Both, table 20 and Figure 34 indicate the best correlation for the model when the

FARR- and the soft-packed plunger is excluded. The correlation coefficient is then about 0.9104 and if we would consider also the FARR plunger as input parameter the correlation coefficient would decrease slightly to 0.9086 meaning a less good correlation. An evaluation of each plunger itself shows also less good correlation compared to the input argument of line two. If we compare the standard deviation of each line we also see the best results for the second line. As a result, the model will only consider the three Harbison-Fischer plunger (table 9) as input results.

6.2.2. Statistical analysis of the modeled data - cont'd

Chapter 6.2.1 plots the model-results if all four plungers are taken into consideration.

This chapter will closely sum-up the model outcome when just the three Harbison-Fischer plungers were used as input parameters.
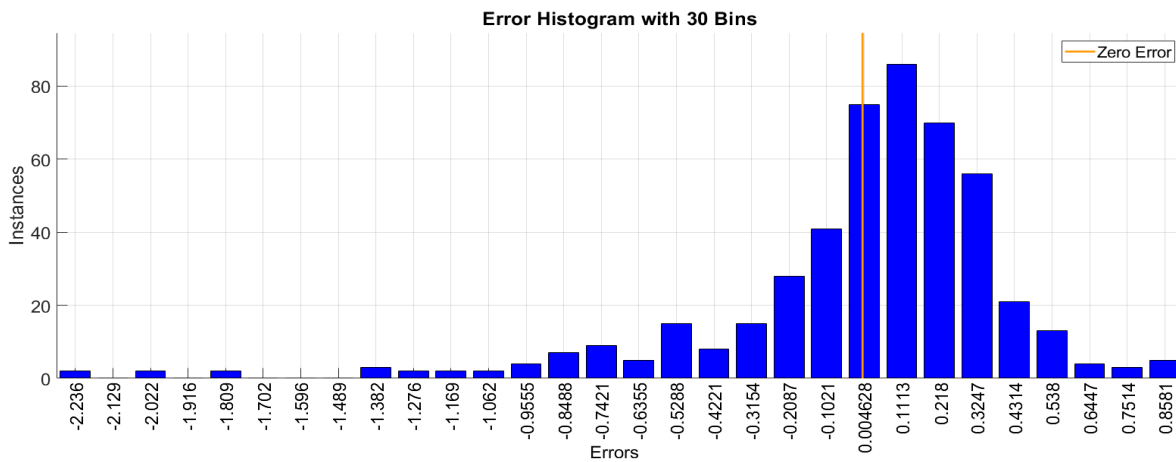
Figure 36: Error distribution for the three Harbison-Fischer plungers
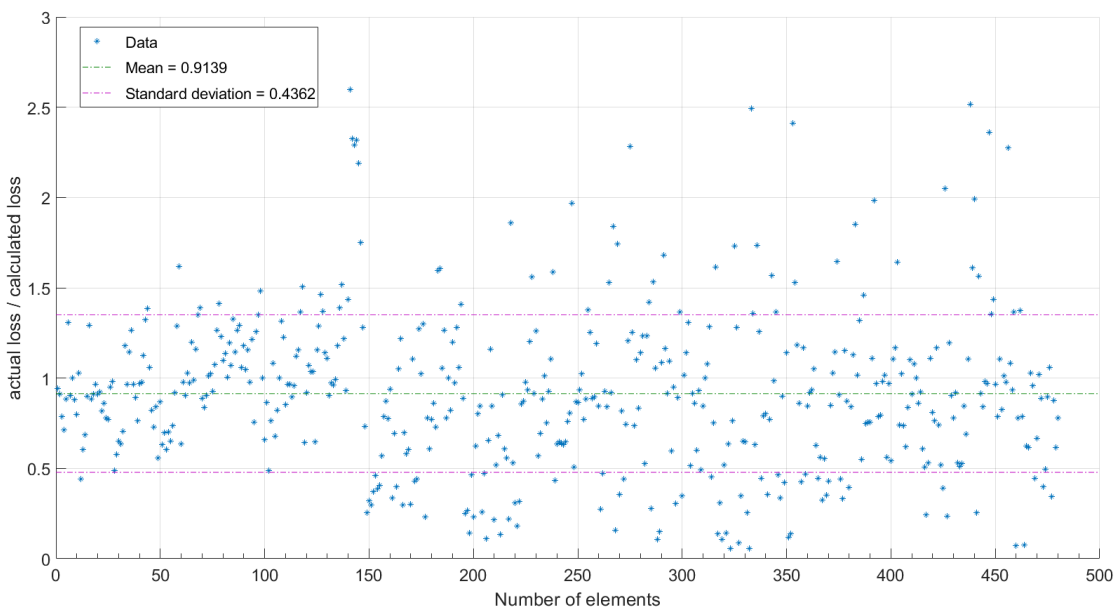
Figure 37: Model error for the three Harbison-Fischer plungers
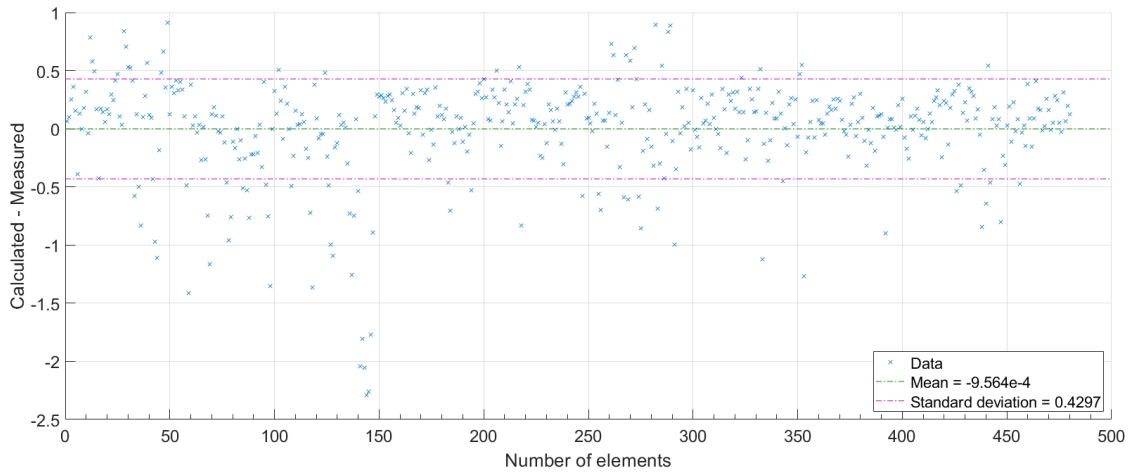
Figure 38: Model error for the three Harbison-Fischer plungers

Figure 36 to Figure 38 display the same calculations as the ones that were made in Chapter 6.2.1, but of course show different outcome.

Figure 37 and Figure 38 clearly differ compared to Figure 34 and 35. The standard deviations are less and the mean for both plots is closer to the desired value. Still, one is able to see the same outliers as in the figures of Chapter 6.2.1. Furthermore, one could see that the calculated error decreased, which means that the model became more accurate.

As a fact of the smaller error and smaller standard deviation of the error, only the three Harbison-Fischer plungers were used to develop the new slippage model. Results of theses plots were summarized in table 20.

7. New empirical slippage model

Result - New model

Goal of this thesis was to establish a model, which is as widely applicable as possible. Such models are hard to develop. The past has shown a variety of slippage models. Models with and without a velocity term, multiplied with coefficients and empirical exponents were used to describe down hole losses.

Every model has its right to be used, since all of them are derived from measurements and are the direct result of an investigative slippage analysis. The difference between each model and approach is linked to the basis of the measurement, the model where it is derived from and the operating conditions. Different assumptions and different approaches lead to different model types.

During the research for this thesis many approaches were studied. The basic slippage model 20 represents the most used approach to describe slippage. Many variations of this model exist, all have different coefficients and exponents. During the research it was then seen, that their is also the necessity to include the plunger velocity as input parameter.

The combination of the old, historical slippage models with the plunger velocity resulted in the following approach:

$$q = (a * v * C * D * t) + b * t * \Delta p * \frac{C^c * D^{4-c}}{\mu^e * L} \tag{63}$$

and with the following variables:

Variable	Value
a	1.7622e+04
b	17.1343
c	1.8203
e	0.3089

Table 21: New model variables

The new model is:

$$q = (17622 * v * C * D * t) + 17.1343 * t * \Delta p * \frac{C^{1.8203} * D^{4-1.8203}}{\mu^{0.3089} * L} \tag{64}$$

The dimension analysis and the old historical model states that the sum of the exponents of $C^x * D^y$ (Clearance times plunger diameter) has to be $x + y = 4$ to match the dimensions. This is why $(C^{1.8203} * D^{4-1.8203})$ the exponent of the plunger diameter is the substraction of $4 - 1.8203$. As mentioned before it was necessary to introduce an exponent for the viscosity. During the evaluation of the data it was recognized, that a model which is derived only with water as a fluid does not model the losses of the modified fluid and vice versa. This made it necessary to add an additional constant. As it can be seen the exponent of the viscosity is 0.3 which decreases the impact of the viscosity on the slippage equation. The model describes the volume loss for the upstroke.

The other coefficients of the model are v as the velocity of the plunger in [m/s], C the clearance in [m], D the plunger diameter in [m], t the time required for one upstroke, Δp is the pressure difference across the plunger in [Pa], μ is the apparent viscosity of the fluid in [Pas] and L is the plunger length in [m].

Applicability

The model is derived under specific operating conditions. The PTF is able to simulate well depths up to 500 meter depth. According to [3] SRP can be used until 16,000 ft (4,877 m) of depth.

Variable		Chambliss [6]	PTF
Discharge pressure	[bar]	120	21 - 37
Intake pressure	[bar]	3.4	2 - 6
Plunger length	[m]	1.219	1.63
Viscosity	[cP]	0.764 (at 90 ° F)	1 - 50 (at around 20 ° C)

Table 22: Chambliss testing conditions vs. PTF testing conditions

As mentioned before the outcome of an equation depends on the input parameters. Making the equation as widely applicable as possible requires a lot and wide spread input parameters.

Table 22 depicts the input parameters of the previous slippage model by Chambliss and the new model derived at the PTF Leoben. What is clearly of interest is the discharge pressure of the pump. In general higher discharge pressures lead to less volumetric efficiency. Therefore the setting depth of the pump under testing conditions has major impact on the result/equation parameters.

The new model is derived for pump outtake pressures up to 40 bars and is probably therefore limited in the loss-prediction for deeper wells with higher outtake pressures. The discharge pressure was varied during the tests compared to the previous models. Previous models are based on real pumps but lack in the variation of setting depth. The discharge pressure of Chambliss's model is three to five times higher than the ones used at the PTF. The ability to predict losses for pumps which are installed shallower is questionable. The new model is therefore best applicable for more shallow wells but maybe lack in precision for deeper wells.

8. Conclusion

An optimally designed well is necessary to increase the production rate, well life time and reduce operating costs. Slippage is required in a certain amount to lubricate the pump and avoid early failure but on the other hand to slippage reduces the volumetric efficiency which makes the well less profitable. An equilibrium between enough lubrication and to much loss is essential for the pump.

Therefore it is necessary to have accurate models to describe slippage losses for sucker rod pumps. The previous published models lack in the variation of input parameters and a general application is therefore limited. The already published models are only applicable for certain operating conditions.

For this thesis it was tried to vary the input parameters as much as possible to establish a model which is applicable as wide as possible.

The comparison between the old and the new model showed a huge difference in loss prediction. One should mention that most of the models are the result of measurements at one specific well with specific operating condition. As in the case of Chambliss [6] the discharge pressure was three to five times higher than the discharge pressure at the PTF. To be able to predict losses with a specific model for every condition is not possible. The model from Chambliss [6] and all other models mentioned above have their applicability for certain operating conditions. So does the model developed at the PTF. The new model is best applicable for more shallow pumps, since measurements were performed for discharge pressures up to 37 *bar*. Fluid viscosity, pump speed, intake and discharge pressure and plunger type have been varied to increase the variety of input parameters.

Goal of this thesis was to establish a model which is applicable for many wells.

$$q = (17622 * v * C * D * t) + 17.1343 * t * P * \frac{C^{1.8203} * D^{4-1.8203}}{\mu^{0.3089} * L}$$

Recommendations

As mentioned above a maximum discharge pressure of 37 *bar* was used to develop the new slippage model. Being able to predict losses for deeper wells is questionable and may result in imprecise predictions. It is recommended to repeat the same test program with higher discharge pressures. This may increase the accuracy to predict losses for deeper wells.

References

[1] Daniel Kochtik. "Systematic Comparison between the Standard Sucker Rod Pump and the SRABS – Pump". Bachelor Thesis. Leoben: Montanuniversitaet Leoben, 2017.

[2] Daniel Kochtik and Clemens Langbauer. "Volumetric Efficiency Evaluation of Sucker-Rod-Pumping Applications Performed on a Pump Testing Facility". In: *SPE Middle East Artificial Lift Conference and Exhibition*. Society of Petroleum Engineers, 2018. DOI: 10.2118/192454-MS.

[3] Takacs Gabor. *Sucker-rod pumping manual*. Tulsa Okla.: PennWell, 2003. ISBN: 0878148922.

[4] Joe Dunn Clegg, ed. *Petroleum engineering handbook*. Richardson, Tex.: SPE, 2007. ISBN: 978-1555631185.

[5] Gang Sheng Chen and Xiandong Liu, eds. *Friction dynamics: Principles and applications*. Woodhead Publishing in mechanical engineering. Duxford, UK: Woodhead Publishing is an imprint of Elsevier, 2016. ISBN: 9780081002858. DOI: 10.1016/B978-0-08-100285-8.00005-5.

[6] Richard Kyle Chambliss. "DEVELOPING PLUNGER SLIPPAGE EQUATION FOR ROD-DRAWN OIL WELL PUMPS". Dissertation. Texas: Texas Tech University, 2005.

[7] American Petroleum Institute. *Specification for Subsurface Sucker Rod Pumps and Fittings: API SPECIFICATION 11AX*. 2006.

[8] J.D. Clegg. *Understanding and Combating Gas Interference in pumping wells*. Ed. by American Petroleum Institute. 1963. URL: https://www.onepetro.org/conference-paper/API-63-149.

[9] Sam Gavin Gibbs. *Rod pumping: Modern methods of design, diagnosis and surveillance*. [United States]: Sam Gavin Gibbs, 2012. ISBN: 0984966102.

[10] Schubert, Reinert, Egberts, Dyck. "Härteprüfung: Hochschule Bremen - University of applied sciences". In: (). URL: http://www.hs-bremen.de/internet/hsb/struktur/mitarbeiter/schubert/lehrveranstaltungen/fert/unterlagen_labor/h__rtepr_fung_fert.pdf.

[11] Herbert Hofstätter. "Artificial lift Systems: Sucker rod pumps & diagnosis: Lecture notes". In: 2018 ().

[12] Langbauer Clemens et al. "Sucker Rod Anti-Buckling System to Enable Cost-Effective Oil Production". In: *Sucker Rod Anti-Buckling System to Enable Cost-Effective Oil Production*. Society of Petroleum Engineers, 2018. DOI: 10.2118/191865-MS.

[13] A. T. Bourgoyne et al. *Applied Drilling Engineering*. Vol. v.2. SPE Textbook Series. Richardson: Society of Petroleum Engineers, 1985. ISBN: 9781555630010. URL: http://gbv.eblib.com/patron/FullRecord.aspx?p=3405014.

[14] Bruce Roy Munson. *Fundamentals of fluid mechanics*. 7. ed. Hoboken, NJ: Wiley, 2013. ISBN: 978-1-118-11613-5. URL: http://www.loc.gov/catdir/enhancements/fy1210/2012011618-d.html.

[15] AMETEK CHANDLER ENGINEERING. "INSTRUCTION MANUAL MODEL 3500 Viscometer and 3500LS+". In: (2012). URL: http://www.chandlereng.com.

[16] Hemphill T., Campos W., Pilehvari A. *Yield-Power Law Model More Accurately Predicts Mud Rheology*. Ed. by Oil & Gas Journal 91. 1993.08.23. URL: https://www.glossary.oilfield.slb.com/en/Terms/h/herschel-bulkley_fluid.aspx.

[17] Charles E. Mortimer and Ulrich Müller. *Chemie: Das Basiswissen der Chemie*. 9., überarbeitete Auflage. Stuttgart: Thieme, 2007. ISBN: 9783134843095.

[18] Milda E. Embuscado, ed. *Functionalizing carbohydrates for food applications: Texturizing and bioactive/flavor delivery systems*. Lancaster, Pa.: DEStech Publ, 2014. ISBN: 978-1-60595-038-9.

[19] L. N. Tao, W. F. Donovan. "Through-Flow in Concentric and Eccentric Annuli of Fine Clearance With and Without Relative Motion of the Boundaries". In: *Transactions of ASME - American society of mechanical engineers* 1955.77 (), pp. 1291–1301.

[20] American Petroleum Institute, ed. *An Evaluation Of The Rate Of Slippage Of Oil Past Oil-Well Pump Plungers*. API-44-025. 1944. URL: https://www.onepetro.org/conference-paper/API-44-025.

[21] James C. Cox, H. Nickens, J. Lea. *Beam Pump Rod Buckling and Pump Leakage Considerations*. URL: http://www.alrdc.com/questions/Q%20and%20A%20Material/SWPSC%20paper%20on%20buckling%20X.doc.

[22] Theta Oilfield Services. *XTOOLS Manual*. URL: https://books.google.at/books/about/XTOOLS_Manual.html?id=jHFUqjddjLkC&redir_esc=y.

[23] Inc The MathWorks. *MATLAB - MathWorks: Documentation*. URL: https://de.mathworks.com/help/index.html.

[24] Inc The MathWorks. *MATLAB - MathWorks: Types of objective functions*. URL: https://de.mathworks.com/help/optim/ug/types-of-objective-functions.html.

[25] Inc The MathWorks. *MATLAB - MathWorks: Unconstrained nonlinear optimization algorithms*. URL: https://de.mathworks.com/help/optim/ug/constrained-nonlinear-optimization-algorithms.html.

[26] George E. P. Box, John Stuart Hunter, and William Gordon Hunter. *Statistics for experimenters: Design, innovation, and discovery*. 2. ed. Wiley series in probability and statistics. Hoboken, NJ: Wiley-Interscience, 2005. ISBN: 9780471718130. URL: http://www.loc.gov/catdir/enhancements/fy0619/2004063780-b.html.

[27] Catherine A. Peters. *Statistics for Analysis of Experimental Data*. Princeton University, 2001.

[28] Bosch Rexroth AG. *Rexroth IndraDyn A: Asynchronous Motors MAD / MAF: Project planning manual R911295781*. URL: https://md.boschrexroth.com/modules/BRMV2PDFDownload-internet.dll/R911295781_10.pdf?db=brmv2&lvid=1206276&mvid=14047&clid=20&sid=81664E92A293185B511E3482C7A2756E.borex-tc&sch=M&id=14047,20,1206276.

[29] SAER ELETTROPOMPE S.p.A. *Home - SAER Elettropompe: SAER ELETROPOMPE*. URL: https://www.saerelettropompe.com/home.

[30] Black Gold Pump & Supply. *Plungers*. URL: http://blackgoldpump.com/Components/Plungers/tabid/104/Default.aspx.

[31] Apergy Corporation. *Rod Lift - Apergy Artificial Lift*. URL: https://www.apergyals.com/products/rod-lift/.

[32] L. L.C. Muth Pump. *Muth Pump | We have the pump for you*. URL: http://www.muthpump.com/.

[33] Sirius-ES Handels GmbH. *Sicherheitsdatenblatt S-ES BIO XG: S-ES BIO XG*. URL: http://www.sirius-es.com/.

[34]   Joel L. Zatz and Steven Knapp. "Viscosity of Xanthan Gum Solutions at Low Shear Rates". In: *Journal of Pharmaceutical Sciences* 73.4 (1984), pp. 468–471. ISSN: 00223549. DOI: 10.1002/jps.2600730410.

[35]   Inc The MathWorks. *MATLAB - MathWorks*. 24.06.2019. URL: https://de.mathworks.com/products/matlab.html.

List of Figures

List of Tables

Nomenclature

API   American Petroleum Institute

CAPEX Capital Expenditure

CAPEX Operational Expenditure

ESP   Electric Submersible Pump

HRA   Rockwell scale "A"

HRC   Rockwell scale "C"

PTF   Pump Testing Facility

RP   Recommended Practices

SPE   Society of Petroleum Engineers

SPM   Strokes per minute

SRABS Sucker Rod Anti Buckling System

SRP   Sucker Rod Pump

SSCEF Sum Squared Error Cost Function

W/O   Without

Appendices

A. Appendix

```matlab
1  function [] = Slippageequation
2
3  %% Import measured data
4  % Input-table arrangement: SPM - DeltaP - Mass - Velocity -
       Diameter - viscosity
5  % SPM ... Strokes per minute
6  % Delta P ... Pressure difference across the plunger
7  % Mass ... Produced mass of liquid per stroke
8  % Velocity ... Plunger velocity
9  % Diameter ... Plunger diameter
10 % Viscosity ... Fluid viscosity
11
12 m1 = load(('plunger5681.mat'));
13 dm1=splitvars(struct2table(m1));
14 dm1.Properties.VariableNames={'SPM','DeltaP','Mass','velocity','d
       ','viscosity','true_viscosity'};
15
16 m2 = load(('plunger5695.mat'));
17 dm2=splitvars(struct2table(m2));
18 dm2.Properties.VariableNames={'SPM','DeltaP','Mass','velocity','d
       ','viscosity','true_viscosity'};
19
20 m3 = load(('plungerNeu.mat'));
21 dm3=splitvars(struct2table(m3));
22 dm3.Properties.VariableNames={'SPM','DeltaP','Mass','velocity','d
       ','viscosity','true_viscosity'};
23
24 M = [dm1; dm2; dm3];
25 plunger = table2array(M);
26
27 %% Pre - Calculations
28 % Import pressure difference and produced volume
29 v = plunger(:,4);% velocity of the plunger in [m/s]
30 d = plunger(:,5); % diameter of the plunger in [m]
31 [l2,~] = size(plunger); % length of the "plunger-array"
32 real = plunger(:,3); % actual mass produced [kg]
33
34 y = plunger(:,7); % viscosity of the fluid in [Pa*s]
35 P1 = plunger(:,2); % pressure diff. across the plunger in [bar]
36 P = P1(:,1)*10^5; % convert DeltaP from [bar] to [Pa]
37 SPM = plunger(:,1); %SPM
38
39 C = ((2.25*0.0254)-d)/2; % clearance in [m]
40 L = 1.63; % length plunger in [m]
41 LS = 1.65; % stroke length in [m]
42 t= 60./SPM; % time required for one stroke in [s]
43
```

```matlab
44  % maximal produceable Volume
45  Volume = d(:,1).^2.*(pi()/4 * LS * ones(l2, 1)*1000);
46  loss = Volume - real; % the actual loss
47  maxVol = Volume(1,1); % the max Volume / Mass
48
49  %% Slippage equation
50  % Objective Function (slippage model)
51  f = @(k) (k(1).*v.*C.*d.*t) + (k(2).*t.*P.*(C.^k(3).*d.^(4-k(3))
        ./(y.^k(4).*L)))
52
53  % Initial starting vector
54  k0 = [124; 0.0026; 3; 0];
55
56  %% fmincon
57
58  target = min(loss(:,1),maxVol); % the maximum error
59
60  % Sum squared error cost function
61  SSECF = @(k) sum((target - f(k)).^2);
62
63  % defining input parameters
64
65  % lower boundary of the output array
66  lb = [-20000,-20000,1 ,-20000];
67
68  % upper boundary of the output array
69  ub = [20000,20000 , 4 ,20000];
70
71  A = [];
72  b = [];
73  Aeq = [];
74  beq = [];
75
76  % non-linear constrained to constrain the outcome of the equation
77  nonlcon = @(k)deal(f(k)-maxVol,[]);
78  options = optimset('MaxFunEvals',Inf,'MaxIter',50000000,...
79          'Algorithm','interior-point','Display','iter', ...
80          'PlotFcn', {@optimplotfval});
81
82  % non-linear programming solver
83  [abc] = fmincon(SSECF,k0,A,b,Aeq,beq,lb,ub,nonlcon,options);
84
85  %% Constants
86
87  a = abs(abc(1))
88  b = abs(abc(2))
89  c = abs(abc(3))
90  e = abs(abc(4))
91   end
```

```matlab
1 function [SPMavg] = dataprocessing
2 %% File used to process data and plot results
3 %specifie specific plunger you want to load
4 m = load(uigetfile('*.mat'));
5
6 m = struct2table(m); % define structure as table
7 m = splitvars(m); % splits the columns
8 m.Properties.VariableNames = {'Time','D05_A','D05_S','D03_A','
      D03_S','AI_14','A1_velocity','A1_Position'};
9
10 %% pre-calculations
11 % convert signal to actual mass [kg]
12 m.Mass = (round(m.AI_14*199.68-6.845+4,2));
13 % apply moving average to smooth the data
14 m.Mass2 = movmean(m.Mass,20);
15
16 % Strokes per minute - convert signal value to actual value
17 m.SPM = abs(round((m.A1_velocity/(1650*2)),1));
18 m.Route = (round(m.AI_10+0.055,2));
19 m.dP = round(m.D05_A-m.D03_A,2);
20
21 %% Plot to define specific range for evaluation
22
23 figure()
24 plot(m.Time,m.SPM), hold on
25 plot(m.Time,m.Mass), hold on
26
27 % pick points
28 [get_x]=ginput();
29 get_x=uint64(get_x);
30 get_x=double(get_x);
31
32 % converting picked points to indices
33 A = table2array(m);
34 [~,idx]=min(abs(A(:,1)-get_x(1,1)));
35 start = idx;
36
37 [~,idx]=min(abs(A(:,1)-get_x(2,1)));
38 ende = idx;
39 dt=ende-start;
40
41 % create new table with defined range
42 m_new=m(start:(start+dt),:);
43
44 %% Plot new attributes
45
46 hold on
47 figure()
48 subplot(2,1,1);
49 yyaxis left
50 plot(m_neu.Time,m_neu.Mass2,'k'), hold on
```

```matlab
51  ylabel('Mass produced [kg]')
52  set(gca,'ycolor','k')
53  yyaxis right
54  plot(m_neu.Time,m_neu.dP,'r'), hold on
55  set(gca,'ycolor','r')
56  grid on
57  grid minor
58  ylabel('Pressure difference across Plunger [bar]')
59
60  yyaxis left
61  subplot(2,1,2);
62
63  plot(m_neu.Time,m_neu.SPM,'k'), hold on
64  ylabel('Plunger velocity [SPM]')
65  ylim([0 11]);
66  yyaxis right
67  plot(m_neu.Time,m_neu.A1_Position,'r')
68  set(gca,'ycolor','r')
69  ylabel('Plunger position [mm]')
70  grid on
71  grid minor
72
73  xlabel('time [s]');
74
75  hold off
76  %% Picking points for data evaluation
77
78  % pick points
79  [get_x]=ginput();
80  get_x=uint64(get_x);
81  get_x=double(get_x);
82
83  %converting picked points to indices
84  A = table2array(m_new);
85
86  [a,~] = size(get_x);
87  Array = zeros((a/2),3);
88  SPMavg = array2table(Array);
89  SPMavg.Properties.VariableNames={'SPM','dP','Avg_Mass2'};
90      for i = 1:2:a
91
92      [~,idx]=min(abs(A(:,1)-get_x(i,1)));
93      start = idx;
94
95      [~,idx]=min(abs(A(:,1)-get_x(i+1,1)));
96      ende = idx;
97
98      dt=ende-start;
99      %new table with defined range
100     neu=m_new(start:(start+dt),:);
101     mc = mode(neu.SPM); %most common value in range
```

```matlab
102
103            %neu.SPM=logical(neu.SPM);
104             toDelete = (neu.SPM~=mc);
105             neu(toDelete,:) = [];
106             size(neu);
107
108            % shift downward for signum-function
109             shift = (max(neu.Route)-min(neu.Route))/2;
110             neu.Route2= (neu.Route -(min(neu.Route) + shift));
111
112             toDelete = (neu.Route2==0);
113             neu(toDelete,:) = [];
114             size(neu);
115
116             signum = diff(sign(neu.Route2));
117             idx = find(signum>0); % search for zeros
118
119            %% Produced mass
120             firstvalueM = neu.Mass2(1); %first value of produced mass
                   / start value
121             indexlastvalueM = size(neu.Mass2); % cummulativ produced
                   mass
122             lastvalueM =  neu.Mass2(indexlastvalueM(1,1));
123            %% Pressure difference
124             D05 = trapz(neu.D05_A)/indexlastvalueM(1,1);
125             D03 = trapz(neu.D03_A)/indexlastvalueM(1,1);
126             dP = D05-D03;
127            %% Result matrix
128             numberofstrokes = size(idx);
129             SPMavg.Avg_Mass2(round(i/2)) = (lastvalueM-firstvalueM)/
                   numberofstrokes(1,1);
130             SPMavg.SPM(round(i/2)) = mc;
131             SPMavg.dP(round(i/2)) = dP;
132         end
133
134  end
```
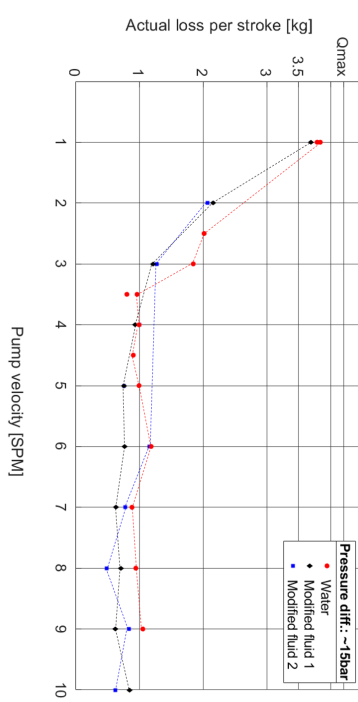
B. Appendix

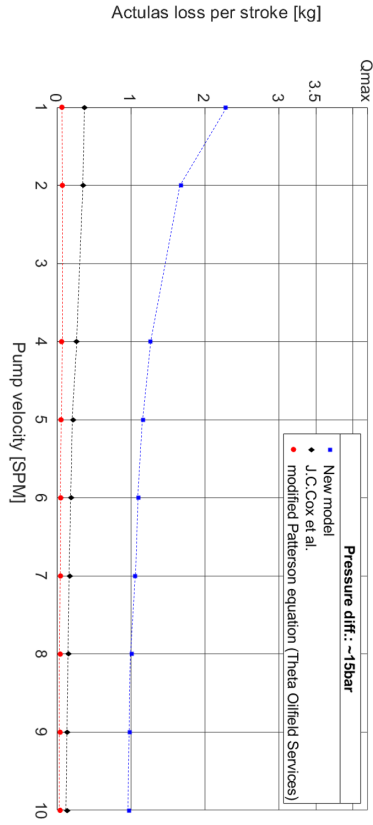(a) Actual losses for 15 bar
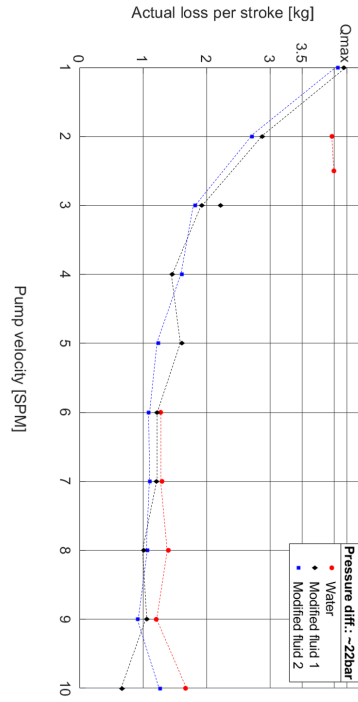
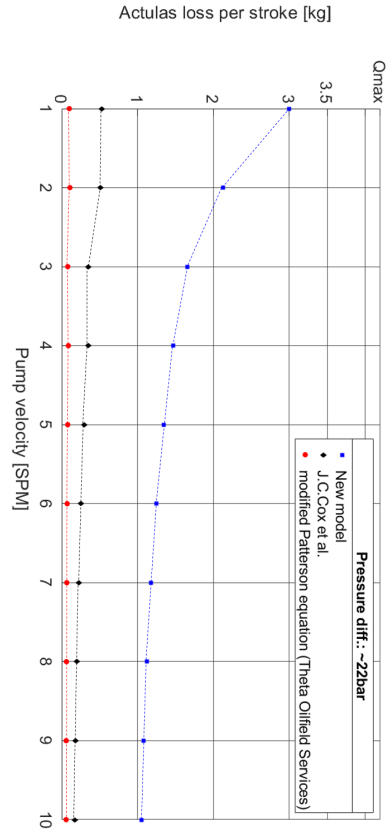(b) Actual losses for 22 bar
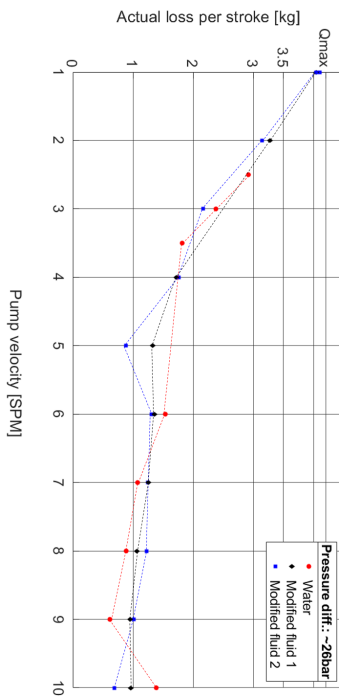
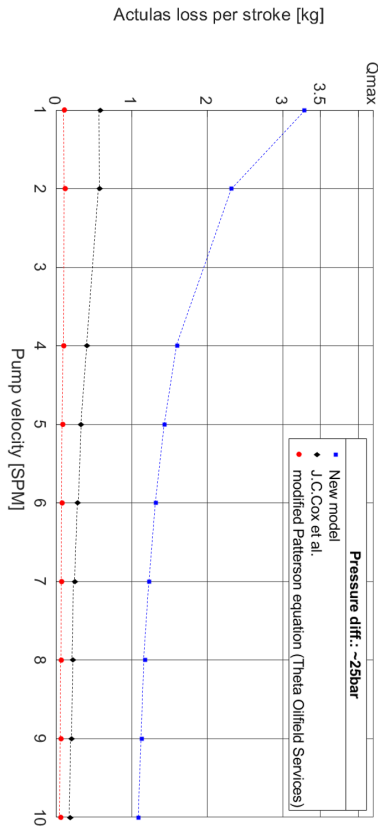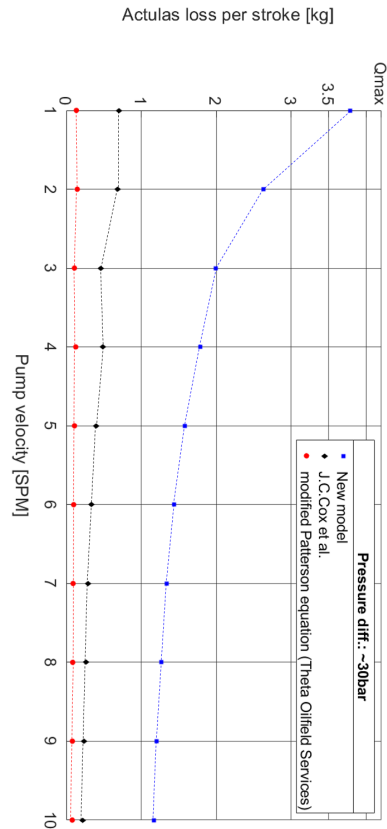(c) Actual losses for 26 bar
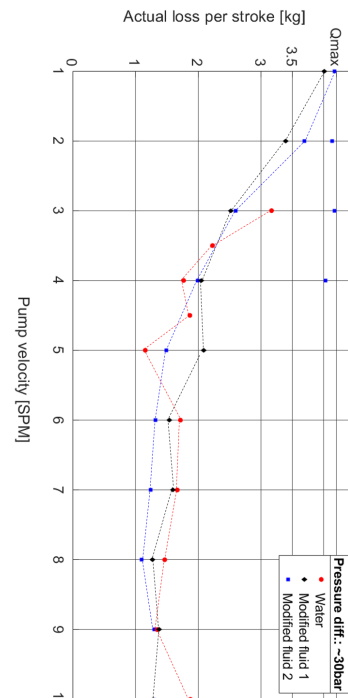
(d) Actual losses for 30 bar

Figure 39: 2D side view of Figure 27

(a) Actual losses for 15 bar

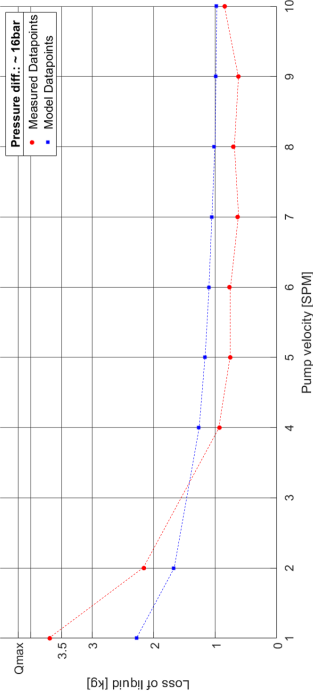(b) Actual losses for 22 bar

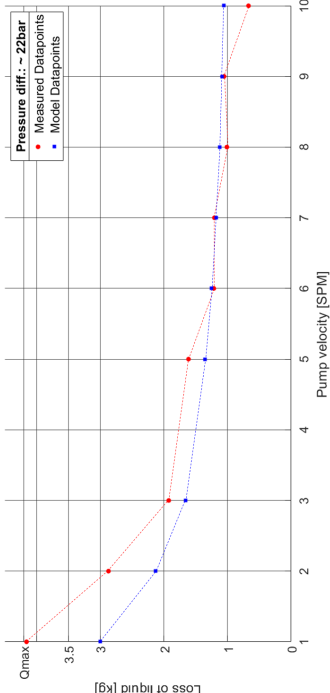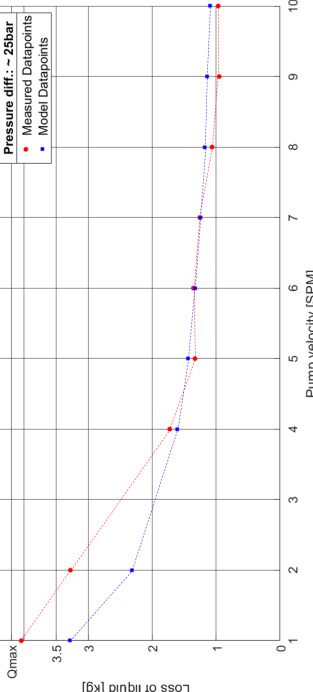(c) Actual losses for 26 bar

(d) Actual losses for 30 bar
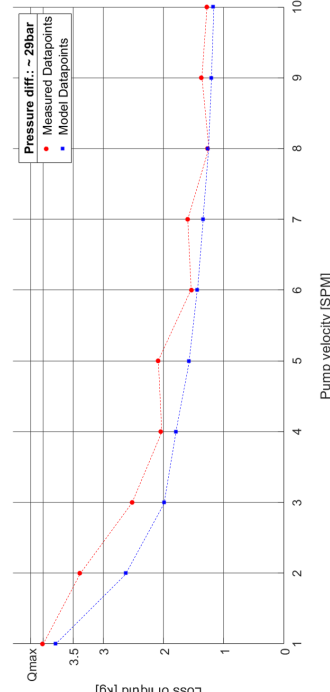
Figure 40: 2D side view of Figure 31 and 32

(a) Actual losses for 16 bar

(b) Actual losses for 22 bar

(c) Actual losses for 25 bar

(d) Actual losses for 29 bar
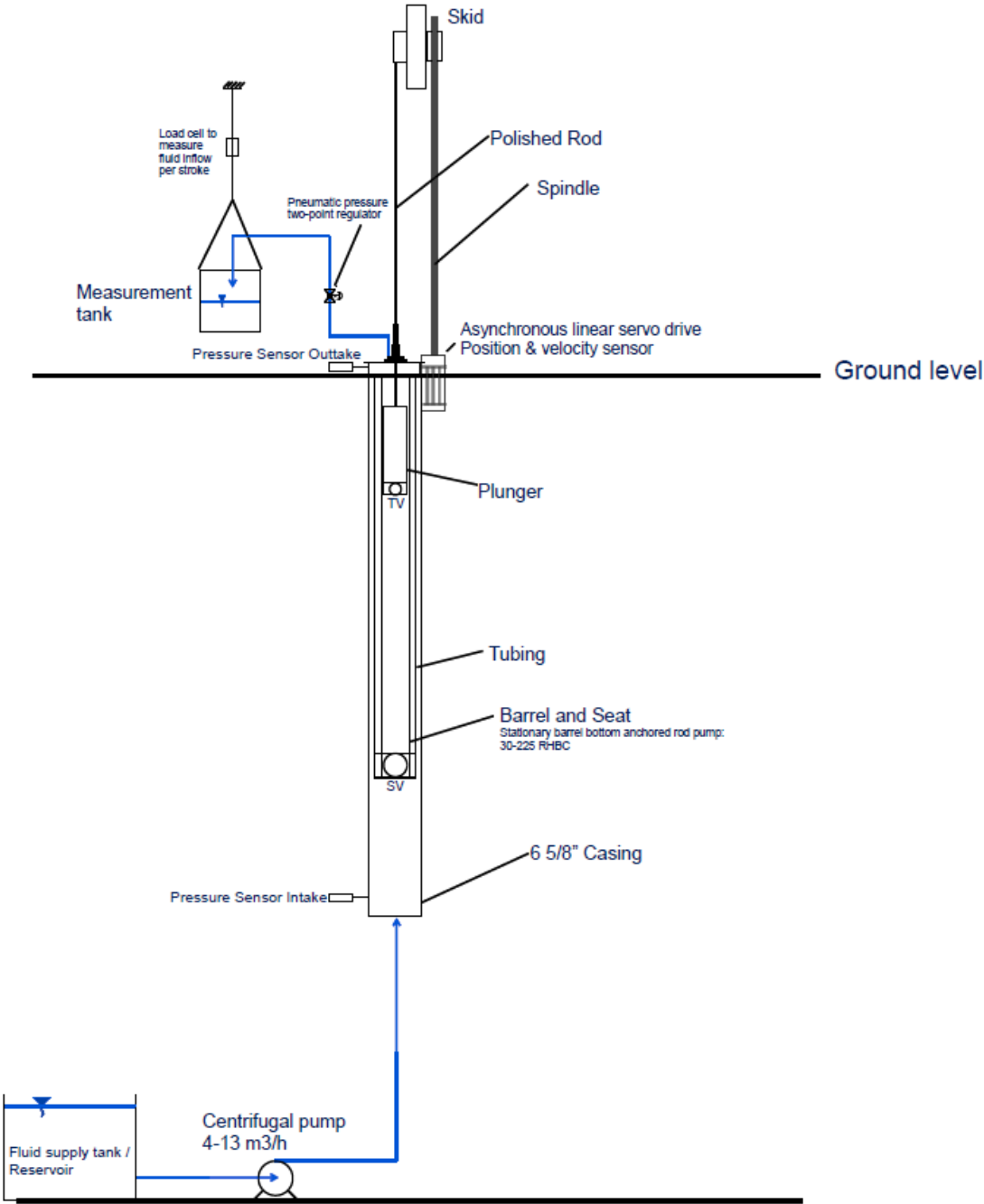
Figure 41: 2D side view of Figure 28

Figure 42: Chandler viscometer 3500M

Figure 43: Pump Test Facility